REVIEW

ADVANCED
ENERGY & SUSTAINABILITY
RESEARCH
Open Access

www.advenergysustres.com

Spin-Selective Catalysts for Oxygen-Involved Electrocatalysis

Haifan Li, Quan Quan, Chun-Yuen Wong,* and Johnny C. Ho*

The sluggish kinetics of oxygen-involved electrolysis, such as oxygen evolution reaction (OER) and oxygen reduction reaction (ORR), hinders the efficiency of the pertaining energy conversion process, which can be promoted by using spin-selective materials to align the spin direction of oxygen-involved intermediates. This review delivers a thorough and timely overview of state-of-the-art spin-selective catalysts for OER and ORR. Primarily, the fundamental principle of spin-selective process is depicted by the spin-sensitive reaction pathways, pointing out that the existence of spin-polarized adsorption sites is necessary for the development of spin-selective catalysts. Subsequently, approaches for investigating the spin-related transition during electrocatalysis are introduced by reviewing in situ technologies and theoretical calculations. Then, the reported spin-selective catalysts are categorized into intrinsic spin-polarized materials, doping-induced spin-polarized materials, and multiple magnetic composites to discuss their application in electrocatalytic OER and ORR as well as their mechanism of spin polarization. Finally, the open questions and prospects in this field are concluded, aiming to offer a clear route for designing novel and highly-efficient spin-polarized materials for industrial oxygen-involved electrocatalysis.

H. Li, C.-Y. Wong
Department of Chemistry
City University of Hong Kong
Hong Kong SAR 999077, China
E-mail: acywong@cityu.edu.hk

Q. Quan, J. C. Ho
Department of Materials Science and Engineering
City University of Hong Kong
Hong Kong SAR 999077, China
E-mail: johnnyho@cityu.edu.hk

C.-Y. Wong, J. C. Ho
State Key Laboratory of Terahertz and Millimeter Waves
City University of Hong Kong
Hong Kong SAR 999077, China

J. C. Ho
Institute for Materials Chemistry and Engineering
Kyushu University
Fukuoka 816-8580, Japan

1. Introduction

Oxygen-involved electrocatalysis (i.e., oxygen evolution reaction [OER] and oxygen reduction reaction [ORR]), pertaining to industrial energy conversation applications, such as water electrolysis,[1–6] metal–air batteries,[7–9] and fuel cells,[10–13] plays a critical role in driving the transition to clean energy and achieving carbon neutrality goals. OER is the bottleneck reaction that occurs at the anode side in water electrolysis to generate oxygen gas, and its sluggish kinetics drags down the overall efficiency. In contrast, ORR occurs at the cathode side of metal–air batteries and fuel cells, turning oxygen gas into water through a redox reaction. Improving the oxygen-involved electrocatalysis process through catalyst design and optimization is essential for enhancing these electrochemical devices' energy conversion efficiency and overall performance. The high energy barrier of OER and ORR originating from the significant size differences among absorbates, such as *OH, *O, and *OOH (* denotes absorption sites), during the four-electron transfer steps hinders the efficiency of electrocatalysis.[14] In the past few decades, numerous researches on developing highly efficient catalysts have proceeded to accelerate the kinetics of OER and ORR, delivering various material design strategies based on increasing the density and intrinsic activity of active sites, such as *d*-electron number,[15] *p*- and *d*-band center,[16,17] e_g orbital filling,[18] *p–d* hybridization,[19,20] charge-transfer energy,[21] etc. Beyond these theories, the recently discovered spin manipulation strategy that controls the spin alignment of oxygen-involved intermediates via spin-selective electron removal received much attention and has been demonstrated to significantly influence the intrinsic activity of spin-polarized catalysts.[22–25]

The spin-sensitivity of OER and ORR reaction pathways is attributed to the distinct spin states of absorbates, such as the singlet *OH and triplet O_2, and the energy consumption is needed to conduct the spin flipping between reaction steps.[26,27] As reported by J. Gracia et al. such a spin-sensitive process can be more efficient by introducing spin-polarized active sites to align the spin direction of oxygen-involved intermediates via quantum spin-exchange interactions.[28–30] In this regard, utilizing spin-polarized catalysts is a promising way to save the energy consumption of spin flipping, thereby lowering the overall electrocatalytic energy barrier.[31–35] Nevertheless, it is difficult for a single material to have both the spin polarization by magnetic ordering and the metallicity

by electronic itineration,[36] and the working temperature of electrocatalysts (usually higher than room temperature) is higher than the Curie temperature of most ferromagnetic (FM) materials. Therefore, constructing materials with coupled spin polarization and metallicity to serve as efficient OER and ORR electrocatalysts is challenging. To address this challenge, a lot of effort has been put into developing spin-selective catalysts. While some reviews in this field have been published in recent years,[24,37,38] few of them classify and review spin-selective catalysts based on the origin of spin polarization within materials, leading to a need for clear guidance for the synthesis of spin-selective catalysts.

Herein, this review delivers a thorough and timely overview of state-of-the-art spin-selective catalysts for OER and ORR. We first depict the fundamentals of the spin-selective process by the spin-sensitive reaction pathways of OER and ORR, which points out that the existence of spin-polarized adsorption sites is necessary for the development of spin-selective catalysts. Subsequently, approaches for investigating the spin-related transition during electrocatalysis are introduced by reviewing in situ technologies and theoretical calculations. Then, the reported spin-selective catalysts are categorized into intrinsic spin-polarized materials, doping-induced spin-polarized materials, and multiple magnetic composites to discuss their application in electrocatalysis and the polarization mechanism (**Figure 1**). Finally, the unresolved questions and prospects in this field are concluded, aiming to offer a clear route for designing novel and highly-efficient spin-polarized toward industrial oxygen-involved electrocatalysis.
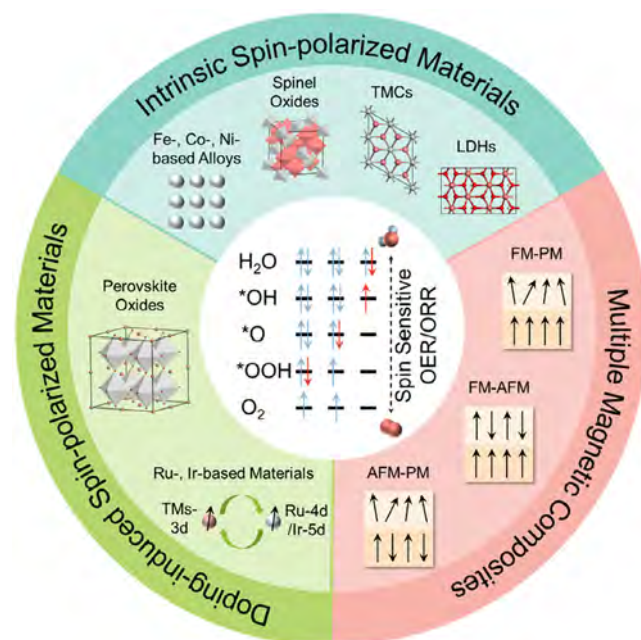

Figure 1. Schematic illustration of spin-selective electron transfer fundamentals for OER and ORR and the reported spin-selective catalysts categorized into intrinsic spin-polarized materials, doping-induced spin-polarized materials, and multiple magnetic composites.

2. Fundamental of Spin-Selective Electron Transfer

2.1. Spin Interaction

Spin, an intrinsic property of angular momentum carried by fundamental particles within the framework of the Standard Model, endows these particles (i.e., fermions and bosons) with a magnetic moment possessing a specific magnitude and orientation. This revelation stemmed from the atomic beam experiments spearheaded by Otto Stern and Walther Gerlach,[39] and was formally solidified with the seminal contributions of Paul Dirac to the realm of relativistic quantum equations.[40] The electron is a kind of fermion with its spin state either spin-up ($\uparrow$) or spin-down ($\downarrow$), corresponding to the spin quantum number of $+1/2$ and $-1/2$, respectively. The Pauli Exclusion Principle and Hund's rules laid the fundamental rules of electron configuration with specific spin states for atoms and ions within the material system, which also results in complicated interaction owing to the intrinsic spin effect among electrons, orbits, and other subatomic particles. These interactions, including exchange interaction, Coulomb repulsion, spin–orbit coupling effect, etc., collectively exert a significant influence on the structure, properties, and chemical behavior of atoms and molecules, thereby playing a vital role in elucidating the formation of chemical bonds, the stability of atoms and molecules, and the advancement of chemical reactions.

In general, similar to energy conservation, a system's total spin angular momentum is also conserved, which means that a chemical reaction is only permissible if the total spin angular momentum of the reactants matches that of the products, resulting in electron and nuclear spin selectivity in reactions.[41] Considering the evolution of intermediates during OER and ORR, the oxygen gas is in a triplet ground state (i.e., the two antibonding π^* orbitals are, respectively, occupied by two electrons with parallel alignment) because of the lower energy of triplet O_2 than singlet O_2 according to Hund's rules, while the spin states of H_2O and absorbed OH^- are singlet with their electrons all paired.[42,43] Therefore, such a process containing the transition between two states of different spin multiplicity should be forbidden. However, the multiple spin interactions among substances provide additional energy levels for spin flipping during chemical reactions, making the reactions possible. Thus, the spin states of catalysts should significantly impact the thermodynamics and kinetics of chemical reactions.[44]

The mechanisms of spin polarization induced by spin interactions are varied by different material systems, and Lee et al. summarized the spin interactions from an intra-atomic to an itinerant system (**Figure 2**).[45] These diverse spin interactions facilitate spin-forbidden OER and ORR processes by modulating the spin states of the intermediates via spin-polarized active sites. Current spin-selective catalysts are primarily based on transition metal elements, such as Fe, Co, Ni, Mn, Cr, Ru, Ir, etc., owing to their strongly correlated d electrons via spin interactions. According to Hubbard model, the correlated electrons within these transition metal-based materials experience competing forces: one pushes it to tunnel to neighboring atoms, while the other pushes it away from its neighbors.[46] From an experimental view, such force can be regulated by alloying, doping,
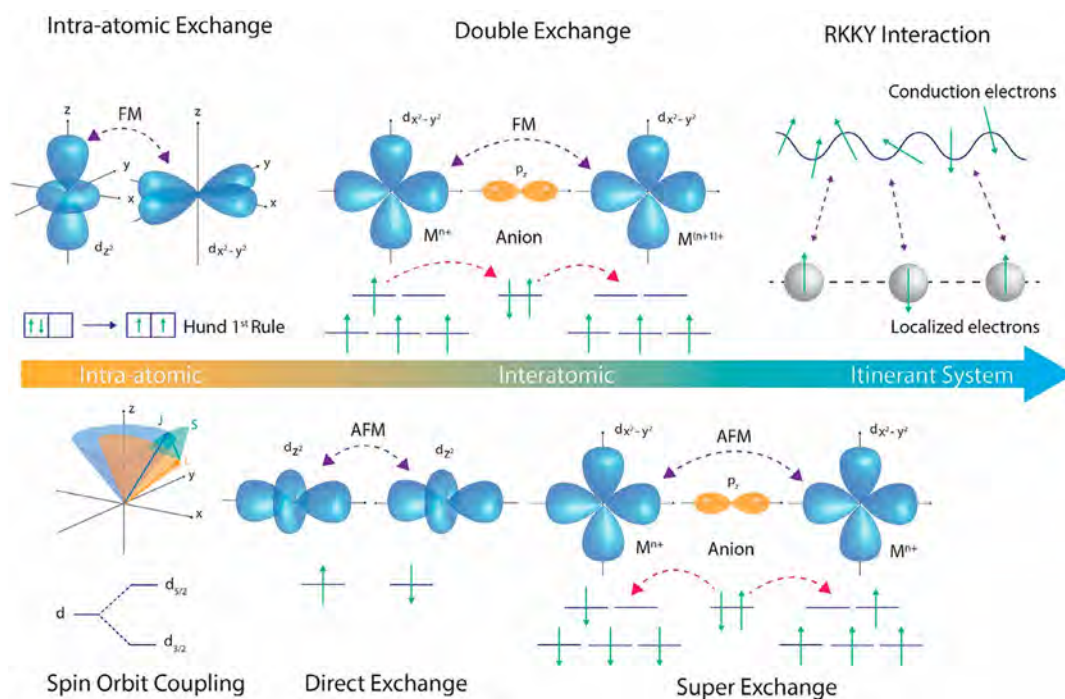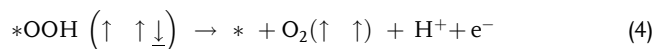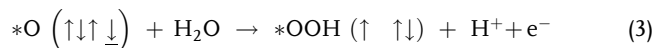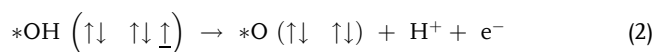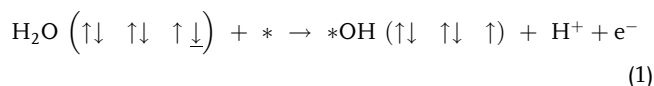
Figure 2. Schematic illustration of various spin interactions from an intra-atomic to an itinerant system. Intra-atomic exchange: the FM exchange (spin alignment) between unpaired electrons on singly occupied orbitals, as is the case of Fe, Co, and Ni metals. Spin–orbit coupling: the interaction of an electron's spin and its orbital motion causes the splitting of electron orbital energy. Double exchange: the FM exchange caused by the interaction between two metal cations of the same element but with different oxidation states through a virtual. Direct exchange: the FM or AFM exchange interaction (dependent on the magnitude of exchange integral J_{ex}) induced by Coulomb repulsion and Paul exclusion principle. RKKY interaction: indirect exchange between localized d-, f-shell electron spins at different locations, mediated by the common exchange interactions with the delocalized conductive electrons. Super exchange is the FM or AFM exchange interaction mediated by anion (e.g., O), as most spinel oxides do. Reproduced with permission.[45] Copyright 2022, American Chemical Society.

heterogenization, etc. to regulate the orbital occupation, spin states, band structure, charge distribution, and so on, which will be discussed in detail in the following sections by specific research cases. As for theoretical calculations, the force is commonly described by correlated energy (U), and its magnitude is crucial for correcting electron correlation, adjusting band structures, simulating robust correlation systems, predicting material properties, and ensuring computational convergence and stability. Choosing the appropriate U value is essential for accurately describing the strong correlation effects and aligning them with experimental observations. Anyhow, spin-related catalysts' properties can be attributed to the intricate spin interactions within the material. It is these interactions that enable numerous spin-forbidden chemical reactions to take place.[47]

2.2. Spin-Selective Pathways of OER and ORR

The reaction pathways of OER and ORR can be typically described by the four-electron reaction process, based on which different reaction pathways have been proposed to explain the catalytic mechanism of various material systems.[48–52] The spin-selective process in oxygen-involved electrocatalysis will be elucidated using the OER pathways under an acidic environment as a representative example, which is shown by the four formulas that represent the reaction steps 1–4 of OER

(the underlined electrons represent the ones to be removal from reactants, the '*' represents the absorption sites, the arrows such as '↑' and '↓' represent the spin direction of electrons):

$$H_2O \left(\uparrow\downarrow \ \uparrow\downarrow \ \uparrow\underline{\downarrow}\right) + * \rightarrow *OH \left(\uparrow\downarrow \ \uparrow\downarrow \ \uparrow\right) + H^+ + e^- \tag{1}$$

$$*OH \left(\uparrow\downarrow \ \uparrow\downarrow \ \underline{\uparrow}\right) \rightarrow *O \left(\uparrow\downarrow \ \uparrow\downarrow\right) + H^+ + e^- \tag{2}$$

$$*O \left(\uparrow\downarrow\uparrow \ \underline{\downarrow}\right) + H_2O \rightarrow *OOH \left(\uparrow \ \uparrow\downarrow\right) + H^+ + e^- \tag{3}$$

$$*OOH \left(\uparrow \ \uparrow\underline{\downarrow}\right) \rightarrow * + O_2(\uparrow \ \uparrow) + H^+ + e^- \tag{4}$$

In step 1, the outer electrons of oxygen within reactant H_2O are paired with hydrogen, and H_2O as well as OH^- are spin-singlets. Through the removal of one spin-down electron from H_2O, the *OH is formed and absorbed on the active sites of catalysts. Then, the unpaired spin-up electron of *OH will be further removed to form *O in step 2. Therefore, it can be seen that the removal of electrons with either spin-up or spin-down orientation in step 1 does not affect the electron spin configuration of the products (i.e., *O) in step 2. The spin-sensitive electron transfer is attributed to the O—O coupling in steps 3 and 4 because a spin-state transition is

**ADVANCED
SCIENCE NEWS**

www.advancedsciencenews.com

**ADVANCED
ENERGY & SUSTAINABILITY
RESEARCH**

www.advenergysustres.com

needed owing to the different spin-state of *O (spin-singlet) and O_2 (spin-triplet). Specifically, in the case of spin alignment, the spin direction of electrons transferred from *O in step 3 is parallel to the ones removed from *OOH, which benefits the formation of triplet oxygen. In contrast, if the two removal electrons in steps 3 and 4 are spin-unaligned, additional energy consumption will be needed to perform spin flipping. Obviously, this spin-flipping step causes additional energy consumption, thus materials with spin-selective functionality will be more efficient than other materials. It has been pointed out that through the quantum spin-exchange interactions, the spin direction of oxygen-involved intermediates (i.e., *O and *OOH) can be controlled by the spin-polarized active sites.[28–30,53] Therefore, to accelerate OER and ORR kinetics from the perspective of spin-selective electron transfer, the primary task is to develop spin-polarized materials with considerable conductivity, intrinsic activity, and ferromagnetism.

Recent progress in developing spin-selective catalysts can be divided into three categories based on the origin of ferromagnetism, which are intrinsic spin-polarized materials, doping-induced spin-polarized materials, and multiple magnetic composites. The catalytic activity of reported spin-selective catalysts herein is summarized in **Table 1**. Most research in this field focuses on common materials with intrinsic ferromagnetism, such as Fe-, Co-, and Ni-based alloys and compounds. However, their intrinsic activity lags behind that of noble metal catalysts.[54,55] To combine the advantages of noble metals and spin-polarization strategy, inducing Ru, Ir-based ferromagnetism by doping is proposed as an effective route to develop highly efficient spin-selective catalysts.[56–58] Additionally, by establishing robust magnetic coupling at the interface between materials with various magnetism, the multimagnetism composites can address the bottlenecks in integrating considerable activity, conductivity, and spin polarization.[59–62]

3. Approaches for Spin-Selective Mechanism Research

3.1. In Situ Experimental Characterization

The application of in situ characterization techniques in electrocatalysis is of paramount significance, through which researchers can monitor in real time the structural evolution of catalytic surfaces, changes in active sites, formation, and conversion of reaction intermediates during electrocatalytic reactions. However, to directly present the transition of spin states for catalytic materials or absorbed intermediates is difficult, and current in situ experimental characterization on identifying spin states during electrochemical reaction includes X-ray absorption spectroscopy (XAS), electron paramagnetic resonance (EPR) spectroscopy, and Mössbauer spectroscopy (MS). Through combing these spin-related technologies with other in situ characterization, such as Raman spectroscopy, infrared spectroscopy, transmission electron microscopy, mass spectrometry, etc., insights into the behavior of catalysts under operational conditions can be obtained, and researchers can precisely tailor more efficient and stable catalysts.

3.1.1. XAS

The in situ XAS is a significant characterization technique used to investigate materials' structure and chemical states.[63] As X-rays pass through a material, the energy within the X-rays is absorbed by the atoms in the material, resulting in the generation of photoelectrons. XAS comprises two primary components as distinguished by their energy position relative to the absorption edge of a specific element: X-ray absorption near-edge structure (XANES, from 30 to 50 eV above the absorption edge) and extended X-ray absorption fine structure (EXAFS, from 50 to 1000 eV above the absorption edge). In the XANES region, X-ray energy is close to the absorption edge, causing inner-shell electrons to be excited to unoccupied orbitals, forming specific shape resonance. The position and shape of the absorption edge provide information about the chemical state of the absorbing atoms and their local environment in the material. In the EXAFS region, after X-rays are absorbed, electrons are excited to higher energy levels and then scatter due to interactions with surrounding atoms. By analyzing the vibrational characteristics of the scattering signals through Fourier transformation or wavelet transformation analysis, multiple details such as atomic distances, coordination numbers, and types of neighboring atoms in the material can be further obtained.

For instance, Oh et al. used in situ near-edge X-ray absorption fine structure (NEXAFS) and Raman spectroscopy to characterize the evolution of spin states for the reconstructed Fe–CoOOH phase during OER (**Figure 3**a).[64] Through iron dipping, sulfur treatment, and restructuring during OER conditions, the CF-FeSO electrode is developed on the basis of cobalt foam (CF). As demonstrated by the results of in situ Raman spectroscopy, the retention of intrinsic OER-active Fe–CoOOH species rather than low-activity CoO_2 under operational OER conditions is confirmed for CF-FeSO (Figure 3b,c). Then, the in situ NEXAFS spectroscopy reveals a moderate increase in the spin states of Co ions during OER operations by comparing the shape resonance associated with t_{2g} orbital occupation (Figure 3d). Specifically, as indicated by the moderate intensity of t_{2g} peaks associated with intermediate spin (IS) state ($t_{2g}^5 e_g^1$), the Co ions undergo a conversion from low spin (LS) state to IS state under operational OER conditions with the existence of Fe^{3+}, rather than transform into high spin (HS) state ($t_{2g}^3 e_g^2$) (Figure 3e). This optimizes the electronic structure and energy of OER intermediates, consequently enhancing OER performance. Analogously, Luo et al. introduced a novel perspective on the significance of the initial spin configuration in metal (oxy)hydroxides in influencing the dynamic generation of active species during the OER.[65] The spin configuration of CoOOH can be effectively controlled via the substitution of transition metals. Through transitioning from LS state into IS state via d–d orbital coupling induced by Mn doping, the Co sites within CoMnOOH are successfully manipulation, as demonstrated by the in situ XAS, Raman spectroscopy, and theoretical calculations. The CoMnOOH displays significant lattice distortion and the highest orbital energy of d_{xy}, resulting in the narrowest energy gap between d_{xy} and d_z^2 orbitals. This structural feature facilitates electron transitions to the d_z^2 orbital, enhances the formation of active high-valent *O–Co(IV) species, and reduces the energy barrier of the rate-determining step.

Table 1. The catalytic activity of reported spin-selective catalysts.

	Catalyst	Overpotential (mV@mA cm^{-2})	Electrolyte	Durability (h@mA cm^{-2})	References
OER	Ni$_1$–MoS$_2$	437@100	1.0 M KOH	NA	[32]
	Cu$_1$–Ni$_6$Fe$_2$–LDH	180@10	1.0 M KOH	50@35	[34]
	Co$_1$–TaS$_2$	330@10	1.0 M KOH	12@20	[35]
	Mn$_{0.4}$Ru$_{0.6}$O$_2$	196@10	0.5 M H$_2$SO$_4$	120@10	[56]
	CoIr	220@10	0.5 M H$_2$SO$_4$	120@NA	[57]
	Mn–RuO$_2$	143@10	0.5 M H$_2$SO$_4$	480@10	[58]
	Co$_3$O$_4$@NiFe–LDH/CC	217@10	1.0 M KOH	24@1000	[62]
	CF-FeSO	192@10	1.0 M KOH	150@100	[64]
		230@100			
	CoMnOOH	256@10	1.0 M KOH	200@10	[65]
	Ce–CoP	240@10	1.0 M KOH	25@10	[77]
	NiGA	340@10	1.0 M KOH	100@10	[104]
	MgFeN$_5$C	224@10	1.0 M KOH	15@10	[107]
	NiFe films	310@10	1.0 M KOH	NA	[109]
	Ni$_3$Fe-CW	266@10	1.0 M KOH	50@10	[116]
	CrMnFeCoNi	315@10	1.0 M KOH	300@10	[117]
	CoFe$_2$O$_4$@NF	323@100	1.0 M KOH	50@20	[118]
	CoFe$_2$O$_4$	522@100	1.0 M KOH	20@10	[119]
	1T-VSe$_2$	228@10	1.0 M KOH	50@24	[121]
	NiCoFe–LDHs	230@10	1.0 M KOH	100@100	[128]
	La$_{0.8}$Sr$_{0.2}$MnO$_3$	120@10	1.0 M KOH	NA	[140]
	La$_{0.7}$Sr$_{0.2}$Ca$_{0.1}$MnO$_3$	540@0.1	1.0 M KOH	6@0.25	

	Catalyst	E_{onset} (V)/$E_{1/2}$ (V)	Electrolyte	Durability (h@mA cm^{-2})	References
ORR	CoNi@NC	0.98/0.86	0.1 M KOH	18@NA	[31]
	High spin Fe(III)–N–C	1.0/0.86	0.1 M KOH	70@20	[74]
	Fe$_{SA/AC}$@HNC	0.88/0.78	0.5 M H$_2$SO4	130@5	[75]
	Co–Er$_2$O$_3$/CNF	0.99/0.83	0.1 M KOH	NA	[78]
	CoFe-NG	NA/0.95	0.1 M KOH	250@5	[96]
	Fe–N–C/S	NA/0.91	0.1 M KOH	NA	[101]
	FeCo-MHs	1.05/0.95	0.1 M KOH	550@20	[106]
	FeCoNi@NC	NA/0.918	0.1 M KOH	8@6.5	[108]

In in situ XAS, setting up specialized electrochemical cells can be intricate and expensive, and changes in electrode materials during reactions may complicate data interpretation. Surface alterations in samples under electrochemical conditions might obscure insights into internal structures. Additionally, the complexity of data analysis and the necessity for specialized expertise to decipher results further compound the challenges. To overcome these limitations, researchers usually integrate in situ XAS with other complementary techniques and theoretical models to gain a more comprehensive understanding of electrocatalytic mechanisms.

3.1.2. EPR Spectroscopy

EPR, or electron spin resonance (ESR), is a spectroscopic technique for studying materials containing unpaired electrons and their spin states (**Figure 4**a).[47,66] The principle underlying EPR spectroscopy involves the interaction between unpaired electrons, an external magnetic field, and microwave radiation. When a sample with unpaired electrons is subjected to a magnetic field, the Zeeman effect causes the electron energy levels to split. This effect arises from the variation in the work required to align the magnetic moment of each electron with the external magnetic field, leading to the splitting of degenerate electronic states. The energy gap between these levels is directly proportional to the strength of the magnetic field. By applying microwave radiation at the resonant frequency matching this energy separation, the unpaired electrons absorb energy and transition between these levels, thus enabling the detection of the EPR signal.

For instance, Hollmann et al. characterized the evolution of magnetism and active phase for mixed cobalt–nickel and cobalt–copper oxides during OER by utilizing in situ Raman
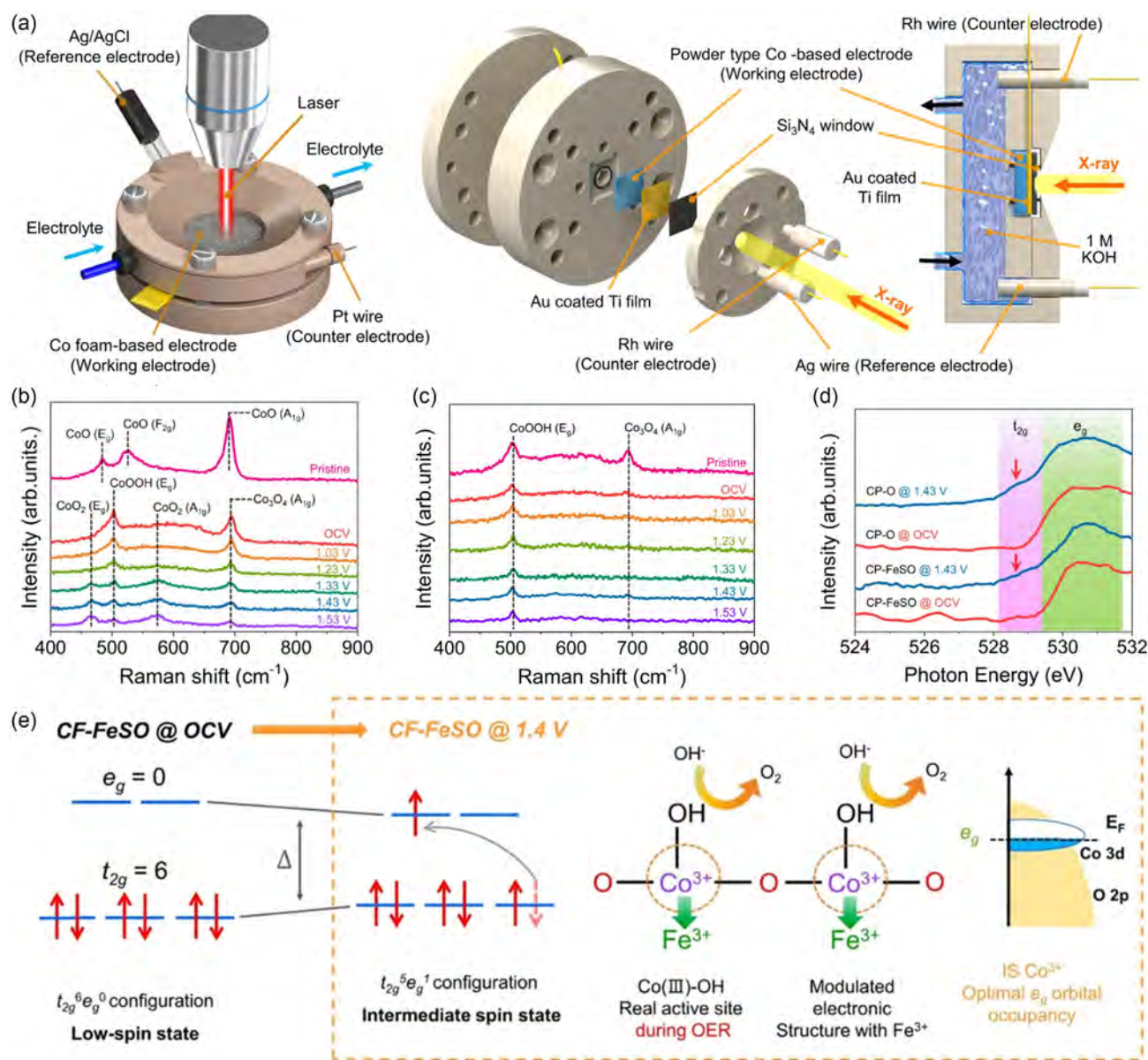
Figure 3. a) Schematic illustration of the in situ Raman spectroscopy and XAS setup. In situ Raman spectrum of b) CF-O and c) CF-FeSO electrodes, respectively. d) In situ Co L-edge NEXAFS spectra of CP-O and CP-FeSO catalysts. e) Spin state under open-circuit voltage and OER conditions, respectively, and the chemical phase and Co $3d$–O $2p$ overlap under OER conditions for CF-FeSO. Reproduced with permission.[64] Copyright 2022, Springer Nature.

spectroscopy and EPR.[67] Their study revealed the formation of γ-NiO(OH) in the less active 2Co1Ni300 catalyst and β-NiO(OH) in the more active 2Co1Ni300p catalyst through in situ Raman analysis of CoNi oxides. This observation suggests that poorly crystalline or amorphous structures, rather than crystalline spinel-type oxides, promote the generation of active NiO(OH) phases. This principle also applies to the CoCu oxide system, where a stable spinel phase impedes OER activity. Furthermore, in situ EPR results highlighted significant structural changes, including partial dissolution of copper and modifications in the antiferromagnetic (AFM) order within the mixed oxide. Interestingly, the spinel phases' alterations in NiCo and

CuCo oxides, along with the emergence of distinct NiO(OH) variants at the onset of OER, were uniquely observable through in situ spectroscopic methods. These modifications are partially reversible upon discontinuing the potential, emphasizing the dynamic behavior of these catalyst systems during OER conditions. In addition, Kutin et al. investigated a cobalt oxide material deposited on a gold electrode that showed efficient water oxidation properties at neutral pH with minimal overpotential.[68] Using in situ EPR technology, they observed the absorption of Co^{2+} from the solution along with tracking the oxidation state of the Co film (Figure 4b). By pinpointing a crucial Co^{4+} intermediate, they could measure its redox potential. Moreover, they
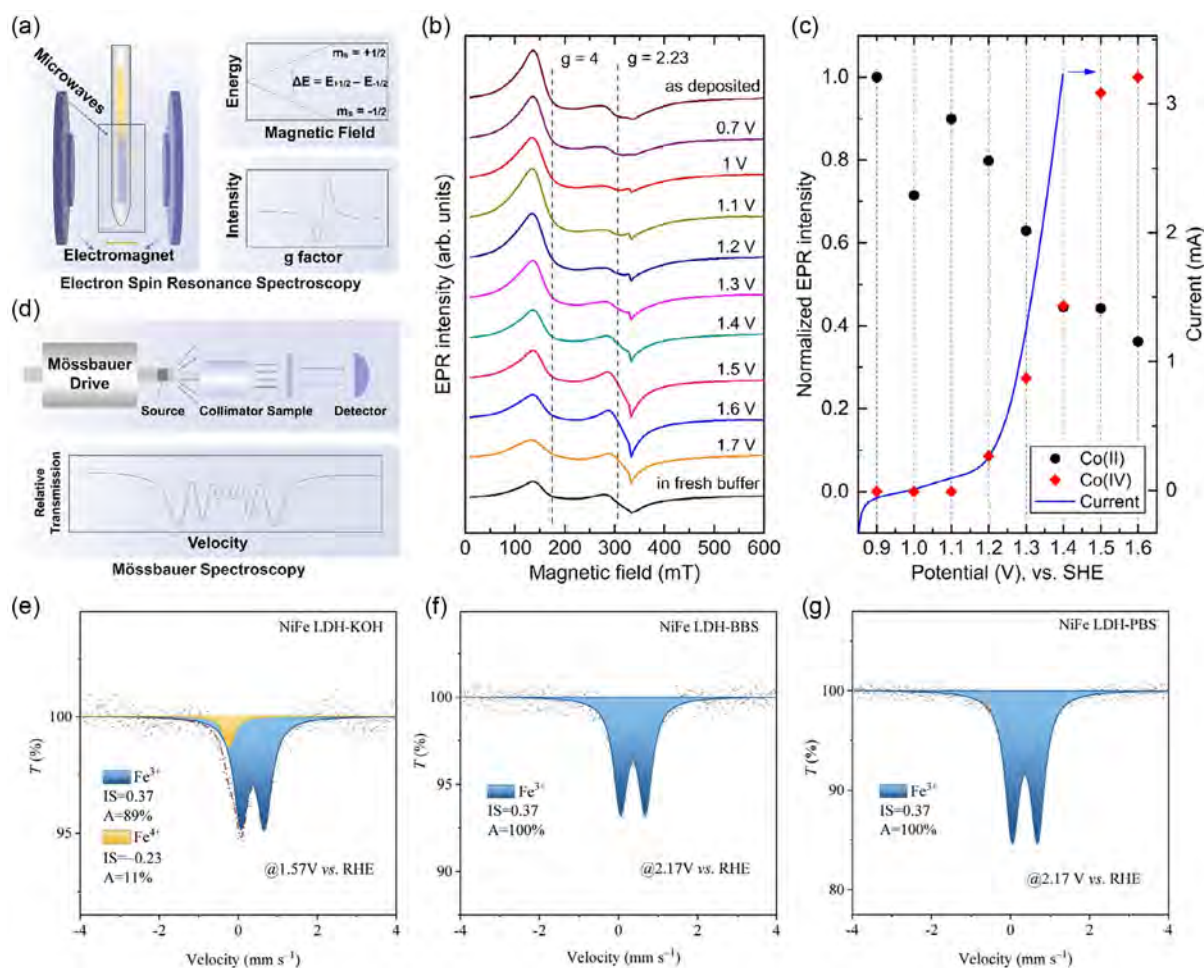
Figure 4. Schematic illustration of a) EPR (or ESR) and d) MS setup. Reproduced with permission.[47] Copyright 2024, Royal Society of Chemistry. b) In situ EPR spectra of the Co–Po-modified working Au electrode electrolyzed at increasing potentials. c) The loss of the Co(II) species (black circles) and the increase in the Co(IV) intensity (red diamonds) as a function of applied potential. Reproduced with permission.[68] Copyright 2019, Multidisciplinary Digital Publishing Institute. The in situ ^{57}Fe MS of NiFe–LDH collected at different pH electrolytes: e) 1.57 V versus RHE, 0.1 mol L^{-1} KOH, pH = 13; f) 2.17 V versus RHE, 0.1 mol L^{-1} BBS (K$_2$B$_4$O$_7$–H$_3$BO$_3$ borate buffer solution), pH 9.2; g) 2.17 V versus RHE, 0.1 mol L^{-1} PBS (KH$_2$PO$_4$–K$_2$HPO$_4$ phosphate buffer solution), pH = 7. Reproduced with permission.[71] Copyright 2023, Elsevier.

interpreted fluctuations in the Co^{2+} signal above 1.2 V as indications of essential localized structural changes necessary for advancing the O—O bond reaction.

For in situ EPR, it has specific limitations that impact its application in various studies. When studying catalysts involved in catalyzing redox reactions (e.g., OER), challenges may arise regarding signal intensity and detection limits. In some catalyst systems, EPR may require higher concentrations to achieve sufficient signal strength, especially when dealing with catalytic activities governed by rare intermediate species. Additionally, EPR often falls short in providing detailed structural information compared to techniques like X-ray diffraction, necessitating the integration of complementary methods for a comprehensive understanding of catalyst structures (e.g., in situ Raman spectroscopy, in situ XAS, etc.). The complex interactions within catalyst systems involving multiple radicals or intricate couplings like dipolar or hyperfine interactions can lead to challenging interpretations of EPR spectra, requiring advanced theoretical

knowledge or computational modeling for accurate analysis. These constraining factors underscore the importance of employing multiple characterization techniques when investigating complex catalyst systems.

3.1.3. MS

MS is a powerful technique used to study the properties of iron-containing compounds (Figure 4c).[47,69] When ^{57}Fe nuclei are subjected to gamma radiation, they can undergo a nuclear transition where they emit or absorb gamma rays at specific energies, which are characteristic of the local chemical environment of the iron atom. This allows researchers to probe the oxidation state, coordination environment, and magnetic properties of iron within a sample. In the realm of catalysis, MS can provide valuable insights into iron oxidation states, the iron species' distribution on the catalyst surface, and the nature of iron-containing

**ADVANCED
SCIENCE NEWS**

www.advancedsciencenews.com

**ADVANCED
ENERGY & SUSTAINABILITY
RESEARCH**
Open Access

www.advenergysustres.com

active sites. This information is crucial for understanding the catalytic mechanisms and optimizing the performance of iron-based catalysts in various reactions.

Nickel–iron oxides/hydroxides are highly potent electrocatalysts for the OER. To unravel the significance of iron in these catalysts, Chen et al. conducted in situ Mössbauer spectroscopic examinations on a 3:1 Ni:Fe layered hydroxide and a hydrous Fe oxide electrocatalyst.[70] These catalysts, synthesized through a hydrothermal precipitation method facilitating direct growth on carbon paper electrodes, revealed the presence of Fe^{4+} species in the NiFe hydroxide catalyst during steady-state water oxidation, constituting up to 21% of the total Fe content. Interestingly, no Fe^{4+} was discerned in the Fe oxide catalyst. While the identified Fe^{4+} species do not directly drive the catalytic activity observed, forthcoming mechanistic hypotheses must consider the availability of this oxidation state of iron within these catalysts. Analogously, Luo et al. employed electrochemical measurements, operando surface-enhanced Raman spectroscopy, and operando ^{57}Fe MS to elucidate the operational mechanism of NiFe layered double hydroxide (LDH) in the OER process across varying pH electrolytes (Figure 4d).[71] Their findings indicate that despite Ni^{3+} and Fe^{4+} species, NiFe–LDH-based electrocatalysts exhibit inferior OER performance in neutral electrolytes compared to alkaline conditions. By integrating electrochemical measurements with spectroscopic inquiries, they illustrated that the rate-determining step of the OER on NiFe–LDH-based electrocatalysts shifts from *O to *OOH in alkaline mediums, whereas *OH formation serves as the rate-determining step in neutral environments.

Limitations of MS include the requirement for samples containing ^{57}Fe, limiting its applicability to iron-containing compounds. It may also be less effective for samples with low iron concentrations or where iron species are highly dispersed, as the signal-to-noise ratio can pose challenges in such cases. Furthermore, interpreting Mössbauer spectra can be complex, particularly when dealing with overlapping signals from multiple iron environments or when the iron atoms exhibit high mobility within the catalyst structure.

3.2. Theoretical Calculations

Density functional theory (DFT) calculations can provide in-depth insights into spin-selective catalysts' thermodynamic and kinetic effects for OER and ORR (**Figure 5**a). Frequently used tools for the theoretical analysis via DFT calculations include difference of charge density, density of states (DOS), band structure, transition state theory, etc. Through the comprehensive utilization of descriptors such as formation energy, adsorption energy, scaling relations, d-/p-band models, orbital occupations, and correlation energy, DFT calculations can provide robust support and guidance for designing efficient catalysts, optimizing reaction conditions, and exploring reaction mechanisms. We refer readers elsewhere for detailed discussions on principles, methods, and mathematical interpretation of various descriptors in DFT.[72] Some progress in investigating the catalytic mechanism of spin-selective catalysts via theoretical calculations will be introduced briefly as follows. Besides the examples reviewed in this section, more research cases on spin-selective catalysts can be seen.

The spin-selective electron removal mechanism during OER can be described by visualizing the difference in charge density and considering the spin direction on specific ions within materials. For example, Xu et al. calculated and compared the spin value of Co and O ions for $ZnCo_2O_4$ and $LiCoVO_4$, respectively, to present the spin-selective conduction channels.[73] For $ZnCo_2O_4$, the Co^{3+} sites are edge-shared, and their electrons are paired with opposing spin directions, resulting in zero magnetization for both Co^{3+} and O sites (Figure 5b). However, in $LiCoVO_4$, the Co^{2+} sites are in HS states with their spin configuration as ($t_{2g}^5 e_g^2$) and the magnetic moment as $\pm 2.66\ \mu_B$ (the direction of magnetic moment is alternated with layer), in which case the edge-shared channels in $LiCoVO_4$ are spin-polarized (Figure 5c,d). In contrast, the ones of $ZnCo_2O_4$ are not spin-sensitive. When operating at a specific potential, the active sites within magnetically aligned pathways can capture electrons oriented by spin from incoming reactants, guiding them along these specialized routes. This action disrupts electron pairs found on the adsorbed molecules, accumulating a suitable magnetic charge at these active sites. Consequently, this sequence supports the creation of triply bonded oxygen molecules, and $LiCoVO_4$ demonstrates superior performance in the OER compared to $ZnCo_2O_4$.

Additionally, Xu et al. proposed that spin-selective electron transfer on the absorption site is crucial for efficient OER for different reaction pathways, which are analyzed through step-by-step adsorption energy calculations (Figure 5e).[61] A crucial step to produce triplet oxygen under the lattice oxygen mechanism (LOM) is creating the $Co^{III}OO\cdot$ intermediate, which requires two oxygen radicals with parallel spins. The oxyl radical triggers spin alignment in the early OER stages. Additionally, aligning two oxygen radicals from different sources before forming the Co^{III}-OO· intermediate shows how spin exchange leads to triplet oxygen production. Without the oxyl radical, aligning oxygen spins incurs an extra barrier, slowing down triplet oxygen formation. High activation energy in the O—O coupling step, when limiting the rate, can be offset by spin-polarized oxyl radicals, enhancing OER activity by reducing the coupling's kinetic barrier. As for the absorbate evolution mechanism (AEM), the spin polarization of oxygen ligands begins with creating the oxyl radical through dehydrogenation. This spin effect helps the O—O coupling step by guiding electrons selectively. During OH⁻ absorption, specific spin directions leave unpaired electrons in ·OH radicals, opposite to Co–O· electrons. Co–OOH prefers paired electrons, aiding O—O bonding. Without Co–O·, pairing π electrons complicates bonding. Creating an oxyl radical with an unpaired electron is crucial for efficient OER. Co–OOH turnover needs electron removal from σ_{O-H} and σ_{M-O} bonds. Spin-selective removal leaves two parallel-spin electrons, aiding O_2 turnover in a triplet state. Without this, a spin flip is required, posing a barrier.

The ORR is the inverse reaction of OER, and generally, the adsorption models of intermediates are the same as OER (i.e., *OH, *O, *OOH). By comparing the changes of Gibbs free energy among intermediate steps by calculating absorption energy, the impact of the spin states of active sites on the energy
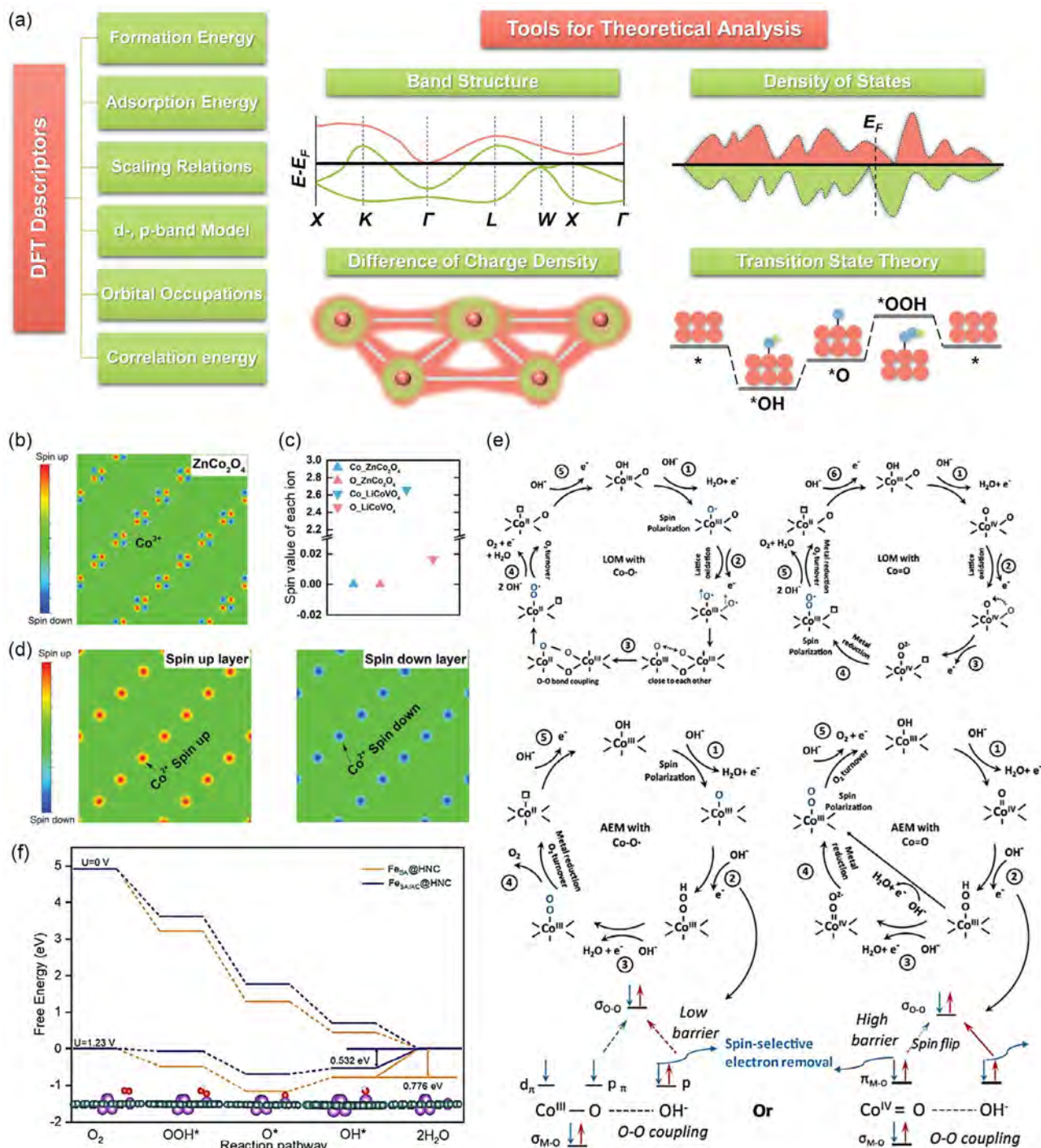
Figure 5. a) Schematic illustration of DFT descriptors and tools for theoretical analysis. b) Spin distribution map of $ZnCo_2O_4$ (111) plane. c) The spin value of Co and O sites of $LiCoVO_4$ and $ZnCo_2O_4$ along the spin channels. d) Spin distribution map of spin-up and spin-down layers in $LiCoVO_4$ along the [001] direction.[73] Reproduced with permission. Copyright 2020, Wiley-VCH. e) Schematic illustration of the LOM and AEM OER pathway for the spin polarization mechanism with Co–O· oxyl radical and Co = O oxo species, respectively. Reproduced with permission.[61] Copyright 2021, Springer Nature. f) Free energy diagram of ORR for $Fe_{SA}@HNC$ and $Fe_{SA/AC}@HNC$ at 1.23 and 0 V versus RHE and schematic ORR process on the Fe−N_4 site of $Fe_{SA/AC}@HNC$. Reproduced with permission.[75] Copyright 2024, Wiley-VCH.

barrier of ORR can be directly depicted. For example, Fu et al. systematically computed the free energy for Fe single-atom catalysts in the LS, MS, and HS states.[74] As the spin state rises, the

occupancy of d_{xz} and d_{yz} orbitals decreases, resulting in the lower occupation of the antibonding orbital after hybridization with O_2, thereby promoting O_2 absorption. The robust interaction

**ADVANCED
SCIENCE NEWS**

www.advancedsciencenews.com

**ADVANCED
ENERGY & SUSTAINABILITY
RESEARCH**

www.advenergysustres.com

between O_2 and high-spin Fe^{3+} can significantly lower the energy barrier of the ORR. Analogously, Wang et al. theoretically confirm the impact of electron spin states on ORR kinetics through DFT calculations (Figure 5f).[75] The introduction of Fe clusters in proximity to $Fe-N_4$ attracts electrons via the nitrogen bridge, altering the interfacial electronic structure of the Fe sites. This leads to the separation of paired electrons in the d-orbital and a transition of the spin configuration to an IS state. This change in spin state reduces the energy barrier for *OH desorption, thereby boosting the catalytic activity of FeSA/AC@HNC during the ORR process, ultimately improving the performance of rechargeable Zn–air batteries.

4. Spin-Selective Electrocatalysts

4.1. Intrinsic Spin-Polarized Materials

Current spin-selective catalysts are usually based on $3d$ transition metal elements such as Fe, Co, and Ni owing to their strong couplings among lattice structure, electronic orbit, and electron spin.[76–80] By combining these elements through alloying, creating spinel oxides, and forming LDHs, a wide array of materials exhibiting original spin-polarization effects can be synthesized as platforms for further exploration. Beyond that some novel transition metal chalcogenides exhibit FM behavior with their Curie point much higher than room temperature, enriching the family of potential spin-selective catalysts.[81,82] To systematically review these spin-polarized materials, we divide this part into Fe-, Co-, Ni-based alloys, spinel oxides, transition metal chalcogenides, and LDH.

4.1.1. Fe-, Co-, Ni-Based Alloys

The alloy family with intrinsic ferromagnetism (e.g., Fe, Co, Ni) is an ideal platform for investigating spin-selective electrochemical reactions. Alloys represent a crucial category of heterogeneous catalysts and usually exhibit notably enhanced catalytic stability, activity, and selectivity compared to their single-metal counterparts.[83] This is because the alloying strategy has effectively reduced the kinetic overpotentials of electrocatalytic reactions by altering the intermediate's absorption on the catalyst surface.[84–86] Based on the complexity of structure and chemical composition, the alloy electrocatalysts can be categorized into single-atom alloys (SAAs),[87–89] polymetallic alloys (PAs),[90–96] and high-entropy alloys (HEAs).[97–100]

At present, several SAAs electrocatalysts utilizing spin-polarization strategy to enhance their performance for OER and ORR in case of the absence or presence of magnetic field assistance have been investigated. Fu et al. prepared a Fe–N–C SAAs catalyst with Cu doping and a controllable magnetic field to regulate the spin state of Fe (**Figure 6**a).[74] Briefly, the Fe- and Cu-contained phthalocyanine solutions are deposited on the substrate by coaxial electrospinning technology to form fibers with a core–shell structure. The inner layer then decomposes, while the Fe/Cu precursors in the outer layer transform into Fe–N and Cu–N, dispersing within the N-doped carbon nanofibers during the ensuing carbonization process, forming Cu-doped Fe–N–C SAAs. The spin state of Fe within Fe–N–C SAAs catalyst

can be regulated from LS to IS and HS by the doping of Cu and applying a magnetic field, leading to the promotion of ORR catalytic activity (Figure 6b,d). Based on the results of DFT calculation, the increasing spin quantum number (S) from LS ($S = 0$) to mediate spin (MS) ($S = 3/2$) and to HS ($S = 5/2$) leads to the incremental atomic magnetic moment from 1.28 to 2.72 and 3.36 μB (Figure 6c). Accordingly, the changes of Gibbs free energy for the rate-determined step (i.e., $\Delta G*_{OOH} = G*_{OOH} - G*_{O_2}$) decrease following the same order of magnetic moment, owing to that the HS state of Fe can optimize the adsorption of triplet oxygen and promote the evolution from $*O_2$ to *OOH.

Analogously, Nowicka et al. studied the impact of applying a magnetic field on ORR performance by inducing the metallic state of Fe within single-atom Fe–N–C catalyst via S-doping and reductive H_2 annealing (Figure 6e).[101] Through controlling the presence of a magnetic field as well as the angle between the working electrode surface and magnetic field, they found that the existence of a magnetic field can improve the catalyst performance owing to the higher selectivity toward ORR rather than its competing reaction (i.e., the production of H_2O_2), which can be further enhanced by setting the angle to 60° (Figure 6f,g). It is worth noting that the influence from the angle of the magnetic field can directly regulate its intersection angle with the electric field to change the Lorentz force and Kelvin force, which was discovered to influence the O_2 gas release during OER.[102] Such spin-polarized active sites optimize the rate-determined O—O coupling step via the selectivity of the spin direction of adsorbed intermediates can also applied to OER, which is the reverse reaction of ORR. Lu et al. reported a FM single-atom catalyst for OER with tunable metal content named Ni_1/MoS_2.[32] Through controlling the Ni content, the Ni_1/MoS_2 exhibits tunable saturated moment with distinct FM behavior due to the realization of long-range magnetic ordering by local magnetic moment from the unpaired $3d$ electron at Ni_{Mo} (III) sites. The gradual enhancement of OER activity by applying an incremental magnetic field is demonstrated by the increasing current density and the more rigorous oxygen gas bubbling at the surface of Ni_1/MoS_2. Further theoretical calculation indicates that the spin alignment of intermediates (e.g., *OH and *O) absorbed on FM active sites tends to be parallel, causing the lowering thermodynamics barrier of rate-determined steps. At the same time, there is additional energy consumption if the absorbed intermediates have antiparallel spin alignment. Similar to the regulation of saturated magnetic moment, Lu et al. also discovered that the spin density modulation by tuning the Co loading in Co_1/TaS_2 can directly influence oxygen adsorption energy.[35] However, too strong or too weak adsorption of intermediates harms the reaction kinetics,[103] and this work reveals the importance of the single atoms loading from the perspective of spin density controlling. Notably, these research works on SAA catalysts also inspire the exploration of single-molecule catalysts (SMCs) with spin-polarized active centers. For example, Sreenivasan et al. anchored $NiCl_2$ on graphene acid to form a highly efficient SMC, and the resultant enhancement in OER catalytic activity under a magnetic field is attributed to the interfacial charge transfer from paramagnetic (PM) Ni center to the substrate and the in situ spin-selective electron transfer (Figure 6h,i).[104]

Compared to SAAs, the additional metal sites in PAs further diversify the approaches of tuning the electronic structure owing
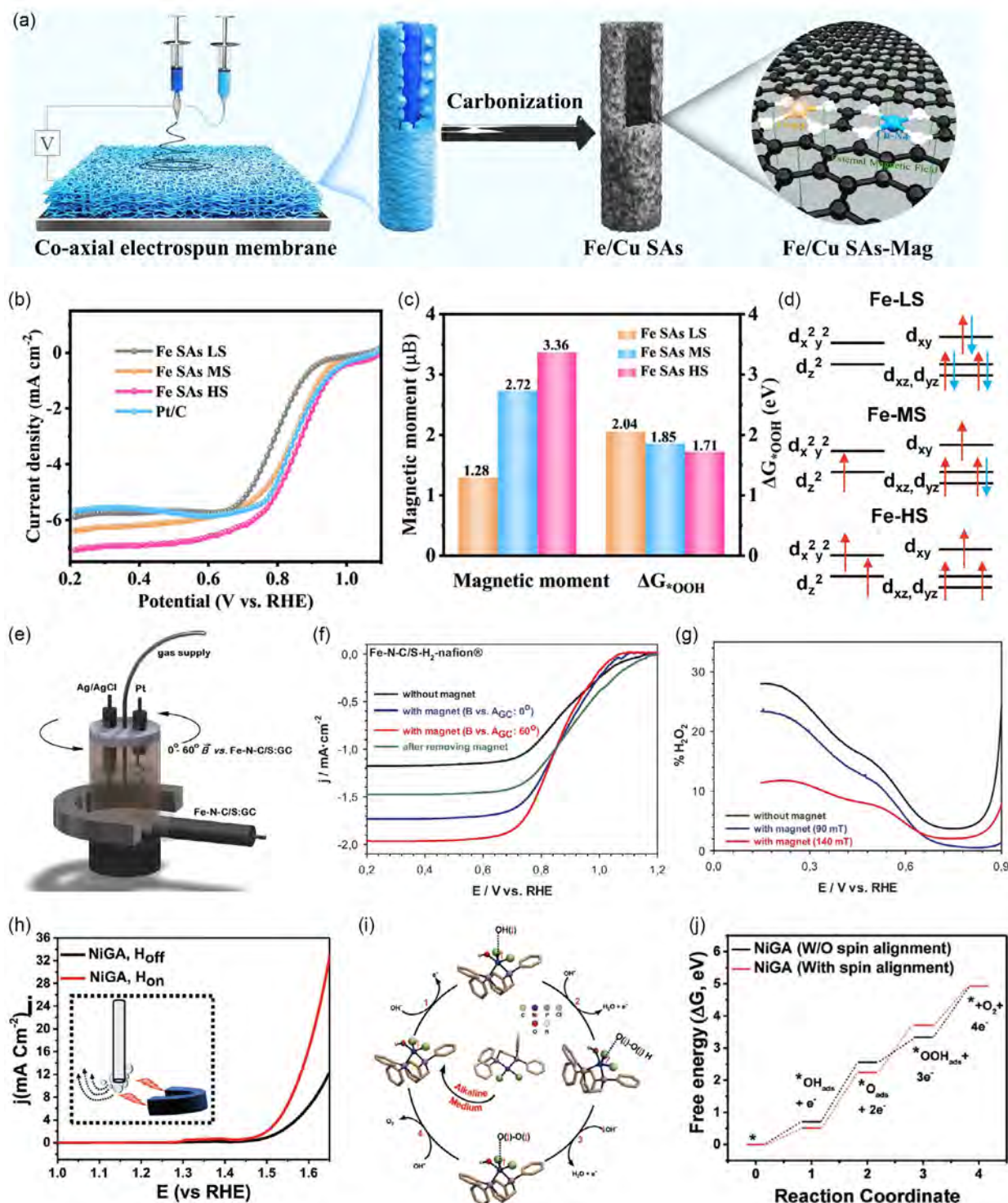
Figure 6. a) Schematic illustration of the synthesis route for the Cu-doped Fe–C–N single-atom catalyst. b) The ORR polarization curves of Fe SAs at LS, MS, and HS, respectively. c) Comparison of magnetic moments and ΔG_{OOH*} for the Fe SAs LS, Fe SAs MS, and Fe SAs HS. Reproduced with permission.[74] Copyright 2023, Wiley-VCH. d) Schematic illumination of Fe spin configuration at LS, MS, and HS. e) Schematic illustration of the electrochemical cell with its angle between the applying magnetic field and the working electrode surface controlled by rotating the cell. f) The ORR polarization curves of Fe–N–C in the presence and absence of a magnetic field and the angle are set at 0° and 60°, respectively. g) Fraction of hydrogen peroxide (%H$_2$O$_2$) produced during ORR. Reproduced with permission.[101] Copyright 2019, Elsevier. h) The ORR polarization curves of NiGA in case of magnetic field's presence (Hon) and absence (Hoff). i) Schematic illustration of the spin-selective OER reaction pathways for NiGA. j) Gibbs free energy plots of NiGA with and without spin alignment. Reproduced with permission.[104] Copyright 2023, Wiley-VCH.

to the greater choice of chemical composition. The PAs can provide a platform to investigate the role of the interaction between metal sites, especially the magnetic coupling effect.[90,105] By the construction of molecular heterostructures (MHs), Chen et al. reported an efficient ORR FeCo-MHs catalyst with diatomic sites to investigate the spin state modulation of Fe and Co sites (**Figure 7**a).[106] Noticeably, the "true" MH is confirmed by rotating the sample platform for atomic-resolution scanning transmission electron microscopy (STEM). The distance between the selected two Fe and Co sites remains unchanged after rotation. This method excludes the "false" information that the photographed atoms can also come from two different surfaces of the carbon support. However, distinct from the monotonic relationship between magnetic moments and ORR performance in SAAs, the overpotential for ORR as the function of magnetic moments in this research indicates that the optimized spin states of Fe and Co sites through MH effect can promote ORR via tuning the binding strength of ORR intermediates toward a suitable level (Figure 7b). Additionally, Hou et al. reported a $MgFeN_5C$ dual-site catalyst with low-spin state Fe sites induced by in-plane square local field deformation via the incorporation of Mg, which can also promote the generation of triplet O_2 through optimizing the absorption thermodynamics.[107] Therefore, to utilize magnetic moments as activity descriptors in PAs, it is more rigorous to consider the modulation effect for each kind of metal site to avoid the misunderstanding obtained from the isolated metal site. The enhancement of OER and ORR catalytic activity by spin-polarized active sites in PAs can also be achieved by applying an external field. Fu et al. prepared a spin-polarized CoNi alloy with an ORR overpotential reduction of 350 mV by applying a magnetic field of 150 mT, which is attributed to the spin-exchange mechanism between metal sites and intermediates to strengthen the p–d hybridization to help spin-selective electron removal (Figure 7c).[31] Analogously, the trimetallic FeCoNi alloy, as reported by Yuan et al. also exhibits distinct reaction kinetics by applying a tunable magnetic field, owing to the efficient capture of oxygen through regulating the spin magnetic moment via electron transfer between multimetal sites (Figure 7d,e).[108]

Different from the above explanation concentrating on the spin-polarized active sites, the origin of magnetic field-enhanced OER catalytic activity can be attributed to the evolution of magnetic domain wall on a larger scale, as reported by Xu et al. in NiFe thin films with intrinsic ferromagnetism (Figure 7f).[109] The density of the magnetic domain wall can be controlled by varying the thickness of NiFe thin films, and the domain walls will disappear with the help of the magnetic field, causing an enhancement in OER activity. The larger enhancement in OER activity is associated with the higher density of the magnetic domain wall, which means a more significant variation in the highly efficient domain area before and after magnetization. This research highlights the role of the magnetic domain size in inducing catalytic activity increment by magnetization, revealing that the existence of a domain wall is the precondition for magnetic field assisting OER. Noticeably, if the scale of materials is small enough, the spin-polarized single-domain catalysts can exhibit the same intrinsic activity without a magnetic field as the magnetic field assisting multidomain catalysts.[33,110] Apart from the alloys prepared on commonly used substrates such as metal

foam, carbon cloth, bulk g-C_3N_4, semiconductor, etc.,[111–115] the sustainable and abundant wood was used to develop Ni_3Fe–wood carbon electrode (CW) PAs with uniform metal ions distribution inside the wood channels by Gan et al. (Figure 7g).[116] The higher charge density around Ni and Fe sites optimizes the O—O coupling step under a magnetic field, which is the reason for enhancing OER catalytic activity (Figure 7h). Moreover, Xu et al. found the improvement of OER performance by magnetic field for CrMnFeCoNi HEAs owing to the spin-selective electron transfer on the spin-polarized metal sites (Figure 7i).[117] Although significant advancements have been achieved in nonprecious metal-based alloy electrocatalysts related to spin, numerous unresolved issues necessitate further investigation. For instance, SAA catalysts exhibiting FM properties have demonstrated spin selectivity to augment catalytic activity in diverse studies, both with and without external magnetic field assistance. Given that single-atom or other atom catalysts are expected to behave as single domains at the atomic scale, the influence of an external magnetic field requires additional elucidation. This demands the synergistic application of complementary in situ characterization techniques to confirm that the external magnetic field alters individual atoms' spin direction or state, thereby impacting their catalytic performance. This integrated approach will not only enhance our understanding of spin-related catalytic mechanisms but also pave the way for developing more efficient and tailored catalysts for various applications. In addition, the relationship between the intrinsic catalytic activity of spin-selective catalysts and their atomic magnetic moment and other magnetic properties needs further clarification. Anyhow, the intrinsic spin-polarization originating from the net magnetic moment of metallic atoms is necessary to serve as spin-selective electrocatalysts for spin-sensitive oxygen-involved electrocatalysis.

4.1.2. Spinel Oxides

$CoFe_2O_4$ is a representative spinel oxide with intrinsic ferromagnetism and has been investigated for spin-polarization-assisted OER under a magnetic field. Xu et al. conducted systematic research on the catalytic activity response of $CoFe_2O_4$ to the magnetic field and its counterparts, such as AFM Co_3O_4 and PM IrO_2 (**Figure 8**a).[23] Through applying the magnetic field beyond the saturation field intensity, the FM $CoFe_2O_4$ exhibits a significant reduction in overpotential. At the same time, the AFM Co_3O_4 and PM IrO_2 show negligible response to the magnetic field (Figure 8b). Since the magnetic ordering within materials is sensitive to temperature, the higher temperature will cause the random spin aligned of atoms, weakening the materials' ferromagnetism. Therefore, it is natural to observe that the overpotential with a magnetic field increases with temperature. The overpotential of $CoFe_2O_4$ gradually decreases owing to the more disordered spin direction of active sites with increasing temperature. Through theoretical calculation, the more efficient OER performance by applying the magnetic field is attributed to the FM exchange between spin-polarized active sites and the electrons on the O p orbitals of intermediates to save the additional energy consumption on spin flipping while generating triplet oxygen (Figure 8c). In addition, the p–d hybridization is also
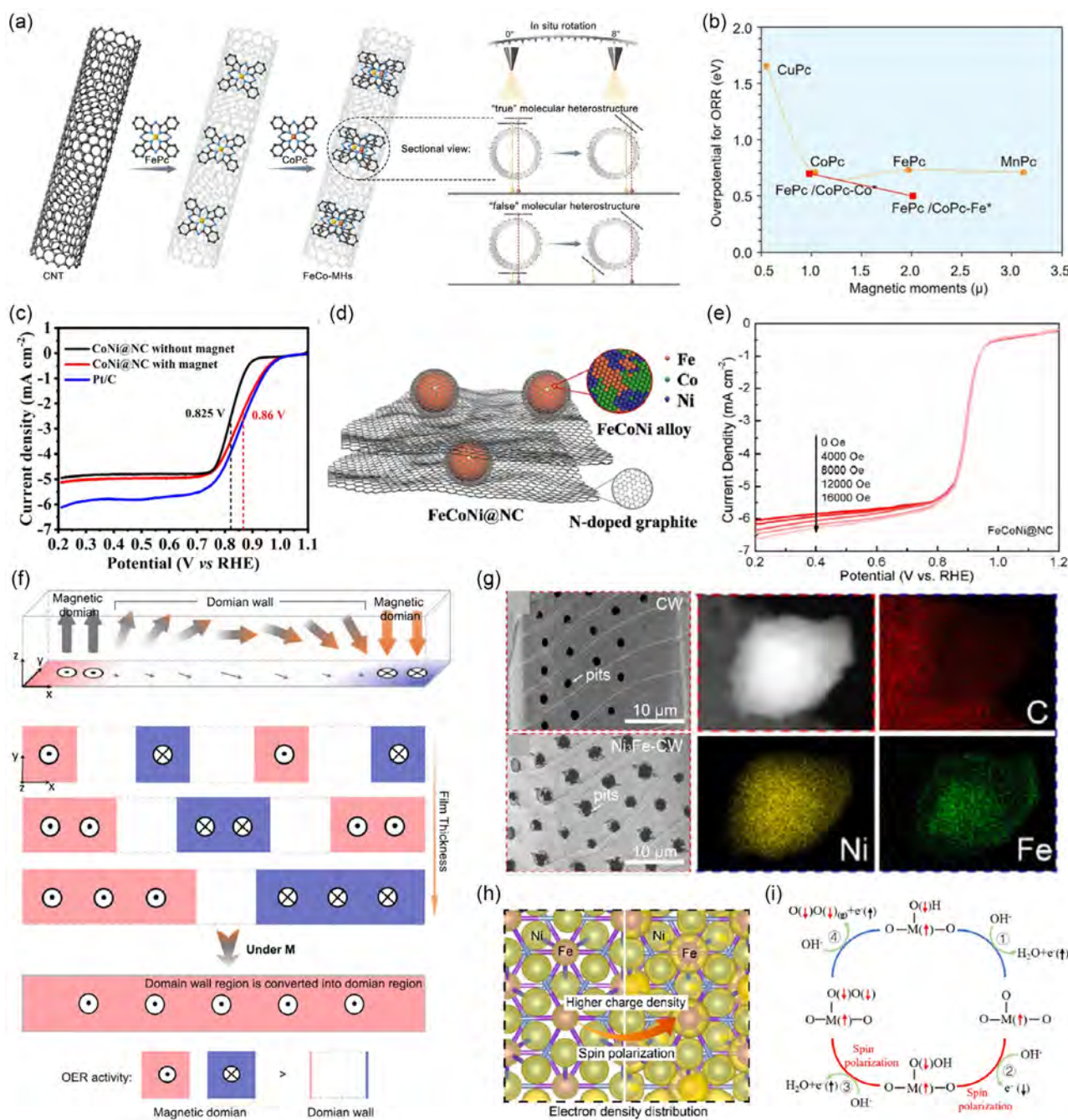
Figure 7. a) Schematic illustration of the MHs design of FeCo-MHs. b) Plots of overpotential against magnetic moment (μ) for ORR. Reproduced with permission.[106] Copyright 2023, American Chemical Society. c) Schematic of the spin-exchange mechanism for the ORR and the LSV curves of CoNi@NC with and without magnetic field. Reproduced with permission.[31] Copyright 2023, American Chemical Society. d) Synthesis protocols of FeCoNi@NC. e) Spin state of Fe^{3+} and Co^{3+} ions and the LSV curves of FeCoNi@NC under various magnetic fields. Reproduced with permission.[108] Copyright 2024, Elsevier. f) Schematic illustration of the evolution of domain wall in NiFe films with different film thicknesses. Reproduced with permission.[109] Copyright 2023, Springer Nature. g) SEM images of pure CW and Ni₃Fe-CW and element mappings. h) The spin density for Ni₃Fe in CW with and without spin polarization. Reproduced with permission.[116] Copyright 2022, Elsevier. i) Schematic illustration of OER reaction mechanism in spin-selective electron transfer pathways. Reproduced with permission.[117] Copyright 2022, Elsevier.

enhanced with spin polarization, as revealed by the difference in charge density (Figure 8d). The spin-polarization effect to enhance OER catalytic activity can be amplified by increasing

the saturation moment of $CoFe_2O_4$ via Fe doping, as reported by Qin et al.[118] This positive correlation between saturation moment and activity enhancement is a universal tendency for
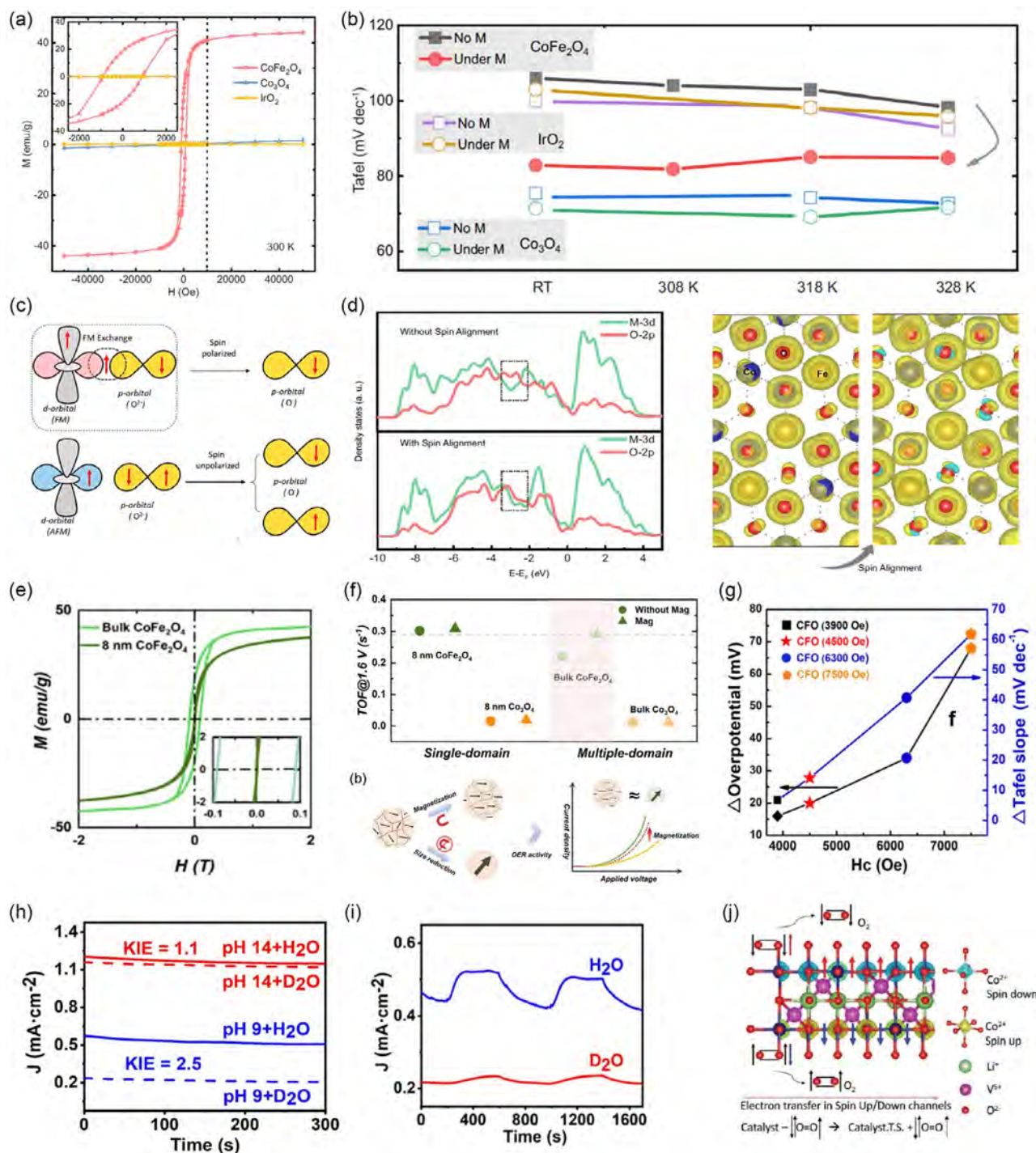
Figure 8. a) The *M–H* loops of CoFe$_2$O$_4$, Co$_3$O$_4$, and IrO$_2$ powders at 300 K. b) Tafel slopes at various temperatures for CoFe$_2$O$_4$, Co$_3$O$_4$, and IrO$_2$ powders in case of the presence and absence of magnetic field. c) Schematic illustration of spin-exchange mechanism for OER. d) The projected DOS (PDOS) and visualized spin density of CoFe$_2$O$_4$ with and without spin alignment. Reproduced with permission.[23] Copyright 2021, Springer Nature. e) *M–H* loops of bulk and 8 nm CoFe$_2$O$_4$. f) The TOF of CoFe$_2$O$_4$ (8 nm and bulk) and Co$_3$O$_4$ (8 nm and bulk) in case of the presence and absence of a magnetic field. The schematic illustration of the OER activity with spin polarization versus single domain. Reproduced with permission.[33] Copyright 2023, Wiley-VCH. g) Comparison of electrochemical performance of CoFe$_2$O$_4$ as a function of coercivity in case of the presence and absence of magnetic field. Reproduced with permission.[119] Copyright 2022, American Chemical Society. h) The chronoamperometry (*i–t*) curves of Fe$_3$O$_4$ at 1.6 V in H$_2$O and D$_2$O and in two electrolytes with different pH. i) The *i–t* curves of Fe$_3$O$_4$ at 1.6 V in H$_2$O and D$_2$O under a switchable magnetic field of 150 mT. Reproduced with permission.[120] Copyright 2023, Wiley-VCH. j) Schematic illustration of spin selective electron transfer in layered AFM LiCoVO$_4$. Reproduced with permission.[73] Copyright 2020, Wiley-VCH.

**ADVANCED
SCIENCE NEWS**

www.advancedsciencenews.com

**ADVANCED
ENERGY & SUSTAINABILITY
RESEARCH**

www.advenergysustres.com

various FM electrocatalysts such as $NiZnFe_4O_x$, $NiZnFeO_x$, $ZnFeO_x$, $Ni_2Cr_2FeO_x$, $FeNi4O_x$, and $NiFe_2O_x$, as investigated by Galán-Mascarós et al.[22] Additionally, by controlling the size of the $CoFe_2O_4$ particle from nanometer to bulk scale, its catalytic activity response to the magnetic field can be further regulated, which is the case reported by Xu et al. (Figure 8e).[33] By comparing bulk $CoFe_2O_4$ and single-domain $CoFe_2O_4$ (8 nm), it is observed that the bulk sample can exhibit an obvious increase in intrinsic activity via turnover frequency (TOF). In contrast, the response of bulk $CoFe_2O_4$ is negligible (Figure 8f). The single-domain $CoFe_2O_4$ (8 nm) can achieve spin polarization without a magnetic field, while the multidomain bulk $CoFe_2O_4$ cannot be self-polarized. As a comparison, the AFM Co_3O_4 has no response to the magnetic field for Co_3O_4 particles (8 nm) and bulk Co_3O_4, indicating that such size-dependent activity enhancement originated from the ferromagnetism within materials. Analogously, such size-dependent magnetization-enhanced OER catalytic activity can also be explained from the coercivity perspective, as Xu et al. reported.[119] The coercivity gradually increased by controlling the grain size of $CoFe_2O_4$ nanoparticles, leading to a larger magnetic domain size and higher reaction kinetics improvement under a magnetic field (Figure 8g). Based on the flexible and intrinsic ferromagnetism of $CoFe_2O_4$, more research can be conducted to disclose further the mechanism of magnetic field enhancing OER catalytic activity.

Apart from $CoFe_2O_4$, other non-noble metal oxides with intrinsic ferromagnetism can also act as spin-selective electrocatalysts for spin-sensitive OER. For instance, Zhao et al. documented a spin-enhanced O–H cleavage for enhancing OER upon Fe_3O_4 within a mildly alkaline electrolyte (pH = 9). This process notably boosts O_2 generation compared to situations in strongly alkaline electrolytes (pH = 14), where the mechanism primarily revolves around spin-enhanced O—O bonding.[120] By employing both H_2O and D_2O in electrolyte preparation, the kinetic isotope effect (KIE) becomes evident in weakly alkaline electrolytes. This observation suggests that the rupture of H-related bonds plays a role in the rate-determining steps of OER under mildly alkaline conditions, with molecular H_2O serving as a reagent. (Figure 8h). In contrast, the KIE at strongly alkaline electrolytes is negligible, which means there is no breakage of H-related bonds. Additionally, the magnetic field dependence of O—H cleavage is further verified by the current density fluctuation with the switching magnetic field in the D_2O-prepared electrolyte (Figure 8i). Therefore, besides the previously reported spin-polarization optimized O—O coupling, the simultaneous occurrence of O—H cleavage is also spin-sensitive and can be promoted using FM materials like Fe_3O_4, enlarging the research scope of spin-sensitive electrocatalysis. In addition to the above FM materials that can provide spin-polarized active sites to interact with intermediates directly, the AFM materials with spin-polarized channels can also promote spin-sensitive OER, which is the case in $LaCoVO_4$ reported by Xu et al. (Figure 8j).[73] The HS configuration of Co^{2+} ($t_{2g}^5 e_g^2$) leads to the polarized channels of edge-shared Co^{2+} octahedra, accelerating the accumulation of appropriate magnetic elements for OER. This finding on AFM materials enriches the family of spin-selective catalysts.

4.1.3. Transition Metal Chalcogenides

To date, certain novel transition metal chalcogenides additionally demonstrate FM characteristics, featuring Curie points well above room temperature, which expands the materials framework of potential spin-selective catalysts. However, research on their application as spin-selective catalysts for OER and ORR is limited. The separate $1T-VSe_2$ nanoparticles are synthesized through pulsed laser deposition in conjunction with rapid thermal annealing treatment on carbon matrix, exhibiting room temperature superparamagnetic with clear FM behavior at high-field region owing to the magnetic single-domain structure (**Figure 9**a), as reported by Wang et al.[121] The $1T-VSe_2$ shows increasing OER catalytic activity with the elevating magnetic field intensity. It indicates its spin-polarization-dependent OER reaction pathways by applying a magnetic field (Figure 9b), similar to other spin-selective catalysts discussed above. Through theoretical calculations, the lower overpotential of $1T-VSe_2$ under a magnetic field is attributed to the spin-aligned electrons on O p orbits via the exchange interaction between oxygen-involved intermediates and spin-polarized active sites, in which case the overall energy consumption of generating triplet oxygen is reduced. Notably, the ferromagnetism of 2D $1T-VSe_2$ can be further regulated by controlling the monolayer morphology and interlayer FM coupling.[122–125] The OER mechanism of $1T-VSe_2$ and other TMCs with intrinsic spin polarization needs further exploration from the perspective of 2D material characteristics.

4.1.4. LDHs

LDHs are a category of anion clays composed of brucite-like host layers and interlayer anions that are well known for their unique layered structure and outperforming properties. NiFe–LDHs have especially been discovered in electrocatalysis, photoactive materials, supercapacitors, etc.[126] Additionally, owing to the unpaired spin single electron on e_g orbitals for Fe^{3+}, Co^{2+}, and Ni^{2+}, the LDHs based on these elements are promising to exhibit enhanced OER catalytic activity by spin-polarization optimized bonding between oxygen intermediates and spin-aligned active sites.[34,45,127] Sun et al. reported iron-group LDHs with enhanced OER catalytic activity by applying a magnetic field (Figure 9c).[128] The ferromagnetic behavior of these LDHs is regulated by the varying element compositions, resulting in the varying response of these LDHs to the applying magnetic field while serving OER (Figure 9d). The spin-polarized Fe sites are demonstrated to be active through in situ Raman characterizations. The concentration of Fe within FeCoNi–LDHs significantly regulates the electronic density distribution around active sites to optimize the absorption of intermediates. To further amplify the enhancement of OER catalytic activity for LDHs, the introduction of Cu dopant to modulate the spin state of Fe^{3+} was investigated by Sun et al. (Figure 9e).[34] It is observed that the Cu dopant acts as the bridge of the exchange interaction between Ni^{2+} and Fe^{3+} to induce distinct ferromagnetism within Cu–NiFe–LDHs by double exchange interaction. After Cu doping, the sensitivity of NiFe–LDHs is largely improved to exhibit a more significant enhancement of OER catalytic activity by applying a magnetic field (Figure 9f).
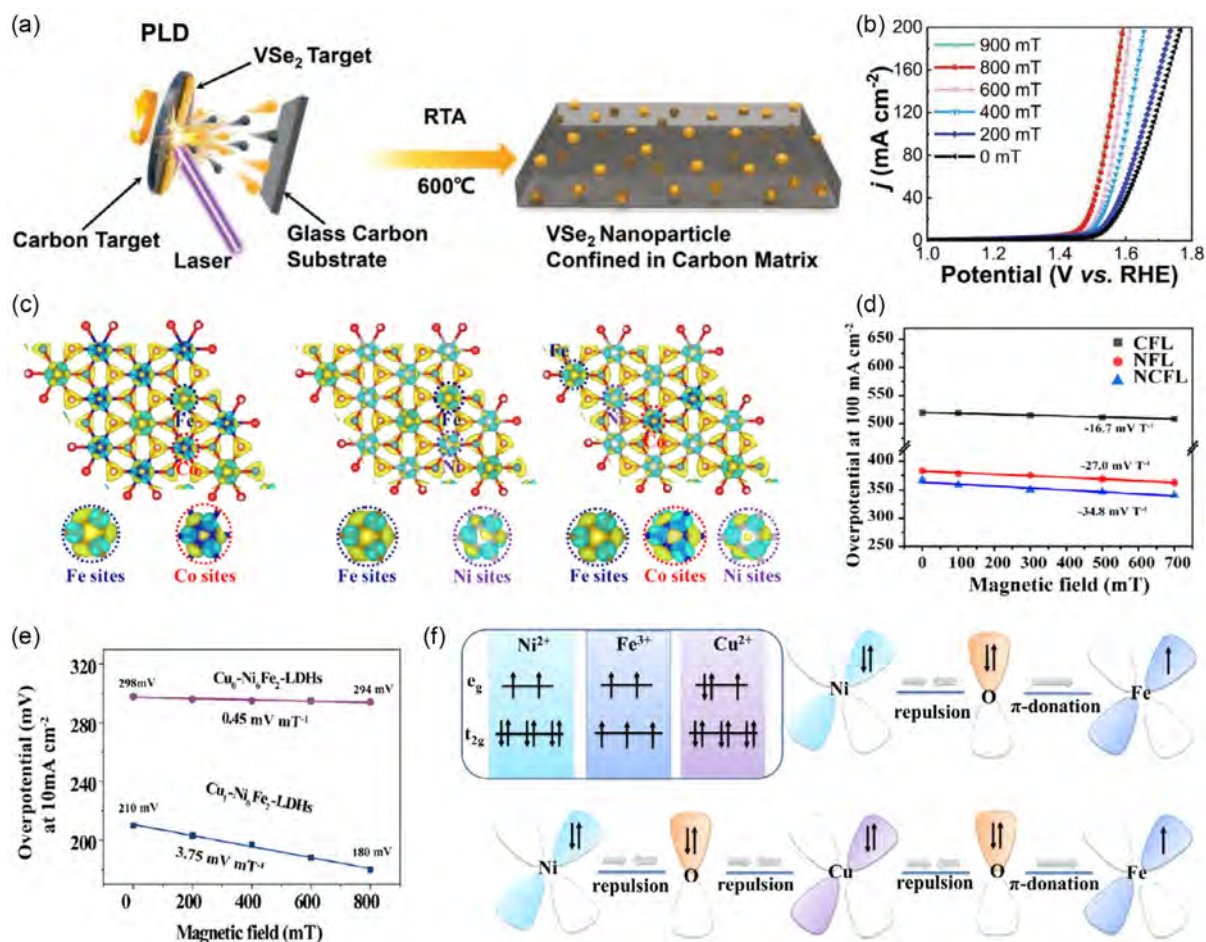
Figure 9. a) Schematic illustration for the synthesis process of confined 1T-VSe$_2$ nanoparticles. b) LSV curves and of 1T-VSe$_2$ nanoparticles under various external magnetic fields. Reproduced with permission.[121] Copyright 2023, Wiley-VCH. c) Differential charge diagram and detailed of central cations for CoFe–LDHs (CFL), NiFe–LDHs (NFL), and NiCoFe–LDHs (NCFL). d) Overpotential−magnetic field curve of CFL, NFL, and NCFL. Reproduced with permission.[128] Copyright 2023, American Chemical Society. e) Overpotential−magnetic field curve of Cu$_0$−Ni$_6$Fe$_2$−LDHs and Cu$_1$−Ni$_6$Fe$_2$−LDHs. f) Schematic illustration of electronic interaction in the d_{xy} orbitals of NiFe−LDHs and Cu−NiFe−LDHs. Reproduced with permission.[34] Copyright 2023, American Chemical Society.

4.2. Doping-Induced Spin-Polarized Materials

Distinct from the 3d transition metal materials with intrinsic spin polarization, the PM, AFM, or diamagnetic materials can be induced into spin-polarized materials via doping. The Ir and Ru elements have 5d/4d electronic orbits. By doping 3d elements, the strong exchange interaction between 3d–5d orbits can induce distinct ferromagnetism within Ir-, Ru-based alloys and compounds. Moreover, some correlated perovskite oxides are also investigated as spin-selective catalysts owing to their tunable electronic structure by doping, expanding their prospects in sustainable energy,[129] in addition to their well-known applications in correlated thermistors,[130–132] biosensors,[133–135] and Mottronic logical devices.[136,137] In this section, we will introduce the spin-selective catalysts with doping-induced spin polarization in the following order of Ru-, Ir-based materials and perovskite oxides.

4.2.1. Ru-, Ir-Based Materials

As reviewed above, current spin-selective catalysts are usually based on 3d transition metal elements such as Fe, Co, and Ni. However, their catalytic activity and durability lag behind the one of noble-metal elements that have outperformed intrinsic activity, such as Ru and Ir. Therefore, inducing ferromagnetism within noble-metal compounds via doping to integrate the superiority of these conventional noble-metal catalysts and the spin-polarization effect is a promising pathway toward highly efficient spin-selective catalysts. Lu et al. reported a CoIr catalyst with an intrinsic spin-polarization effect for serving OER at acidic electrolytes with magnetic field assistance.[57] Through utilizing the robust exchange interaction between 3d and 5d orbits, the 5d Ir element with empty orbitals can be converted from a nonmagnetic metal into a spin-polarized electrocatalyst via alloying with 3d Co element to induce spin–orbit coupling interactions

(**Figure 10**a,b).[34,138,139] It is worth noting that apart from alloying with Co elements, Lu et al. also reported MnIr and NiIr alloys following the same spin-polarization strategy as CoIr with various degrees of ferromagnetism, leading to their different response of overpotentials to the magnetic field (Figure 10c). After DFT calculations, the most significant FM behavior of CoIr alloys as compared to MnIr and NiIr is demonstrated by the results of integration spin-up and spin-down DOS, in which case the net magnetic moments of CoIr are larger than MnIr and NiIr (Figure 10d).

Another potential catalyst for acidic OER is RuO_2. Nevertheless, the poor stability of the Ru element is the primary factor limiting its utilization as an electrocatalyst owing to the high oxidation state of hydrosoluble RuO^{4+} in an acid environment, and much attention has been paid to addressing this problem. To induce ferromagnetism within RuO_2 by element doping, its durability and activity can be optimized. For instance, Shao et al. reported a spin-polarized Mn doping RuO_2 nanoflake as an efficient acidic OER catalyst by establishing the FM exchange interaction between Mn^{2+}/Mn^{3+} and Ru^{4+}/Ru^{5+} based on the Goodenough–Kanamori rule (Figure 10e,f).[58] Notably, the Mn–RuO_2 under a magnetic field exhibits much better catalytic activity and long-term stability than pure AFM RuO_2 and Mn–RuO_2 without a magnetic field. Analogously, Luo et al. also prepared an $Mn_{1-x}Ru_xO_2$ solid solution with its spin polarization explained from the perspectives of spin symmetry broken (Figure 10g).[56] Specifically, the Ru—O—Ru bonds within pure rutile RuO_2 are 101° and 128°, respectively, close to the bond angle of 90° that can generate robust FM exchange, which is in agreement with its destructible itinerant antiferromagnetism at room temperature. Therefore, introducing Mn dopant induces the asymmetry within $Mn_{1-x}Ru_xO_2$, leading to spin-density redistribution around Ru^{4+} by ferromagnetically interacting with spin-polarized Mn sites. The as-prepared can even work at 1 A cm^{-2} for proton exchange membrane water electrolysis in the acidic electrolyte.
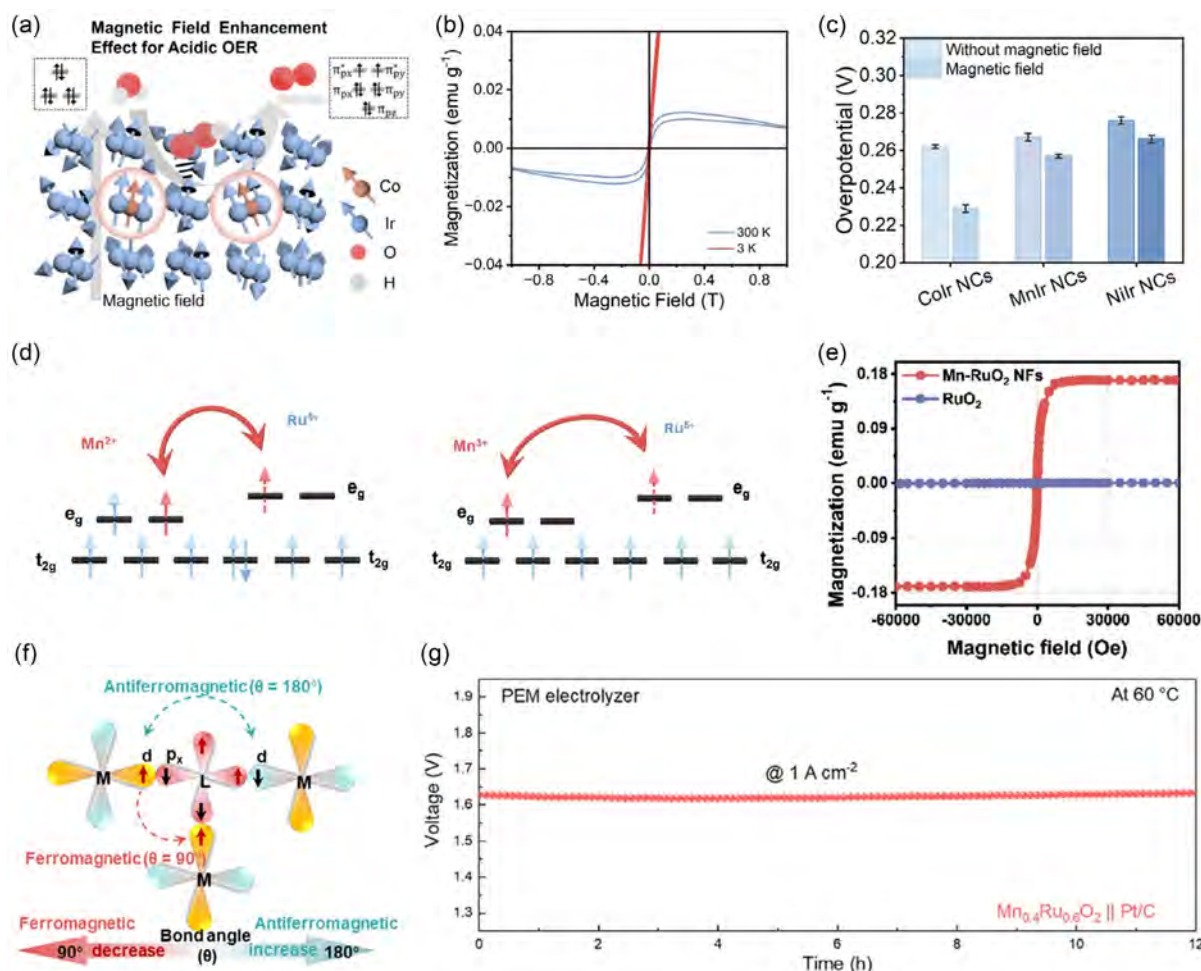

Figure 10. a) Schematic illustration of spin-polarization effect to promote the generation of triplet oxygen for CoIr alloys. b) The *M–H* loops of CoIr NCs at 3 and 300 K. c) Comparison of the overpotential for CoIr NCs, MnIr NCs, and NiIr NCs with and without a magnetic field. Reproduced with permission.[138] Copyright 2024, American Chemical Society. d) Schematic illustration of the FM exchange between Mn^{2+}/Mn^{3+} and Ru^{4+}/Ru^{5+}. e) The *M–H* loops of Mn—RuO_2 NFs and RuO_2 at room temperature. Reproduced with permission.[58] Copyright 2023, Wiley-VCH. f) Schematic illustration of bond angles in FM and AFM structures. g) Chromatopotentiometry curves for $Mn_{0.4}Ru_{0.6}O_2$ at 1 A cm^{-2} at 60 °C. Reproduced with permission.[56] Copyright 2024, American Chemical Society.

4.2.2. Perovskite Oxides

The Mn-based perovskite family is well known for its magnetoresistance effect. Through A-site substitution, the double exchange interaction in Mn^{3+}–O–Mn^{4+} can induce its transition from an AFM insulator to a FM half-metal. This magnetoelectrical transition makes Mn-based perovskite an ideal platform to investigate the relationship between the spin behavior of materials and their catalytic performance. Gao et al. prepared $La_{1-x}Sr_xMnO_3$ with room-temperature FM and magnetoresistance behaviors and investigated its OER catalytic activity under a magnetic field for rechargeable Zn–air battery (**Figure 11**a).[140] The magnetic application can significantly promote the intrinsic activity of $La_{1-x}Sr_xMnO_3$, and the variation of applied potential exhibits a positive correlation with the switchable magnetic field (Figure 11b). On the one hand, the magnetic field-induced magnetoresistance effect declines the resistance of $La_{1-x}Sr_xMnO_3$, reducing charge-transfer resistance and achieving better OER kinetics. On the other hand, the spin-polarized Mn sites significantly cut down the energy consumption of intermediates evolution between *OH and *OOH steps by optimizing the O—O coupling via spin-selective electron transfer (Figure 11c).

Similarly, Lv et al. reported another Mn-based perovskite spin-selective catalyst $La_{0.7}Sr_{0.2}Ca_{0.1}MnO_3$ with its Curie temperature higher than $La_{0.7}Sr_{0.3}MnO_3$ by Ca doping (Figure 11d).[141] The source of ferromagnetism is illustrated by the double exchange interaction model between Mn^{3+} and Mn^{4+}, in which case a spin-up electron from oxygen moves to the empty orbit of Mn^{4+} so that it can receive another electron from Mn^{3+}, leading to the overall effect of electron transfer from Mn^{3+} to Mn^{4+} (Figure 11e). By increasing temperature, the catalytic
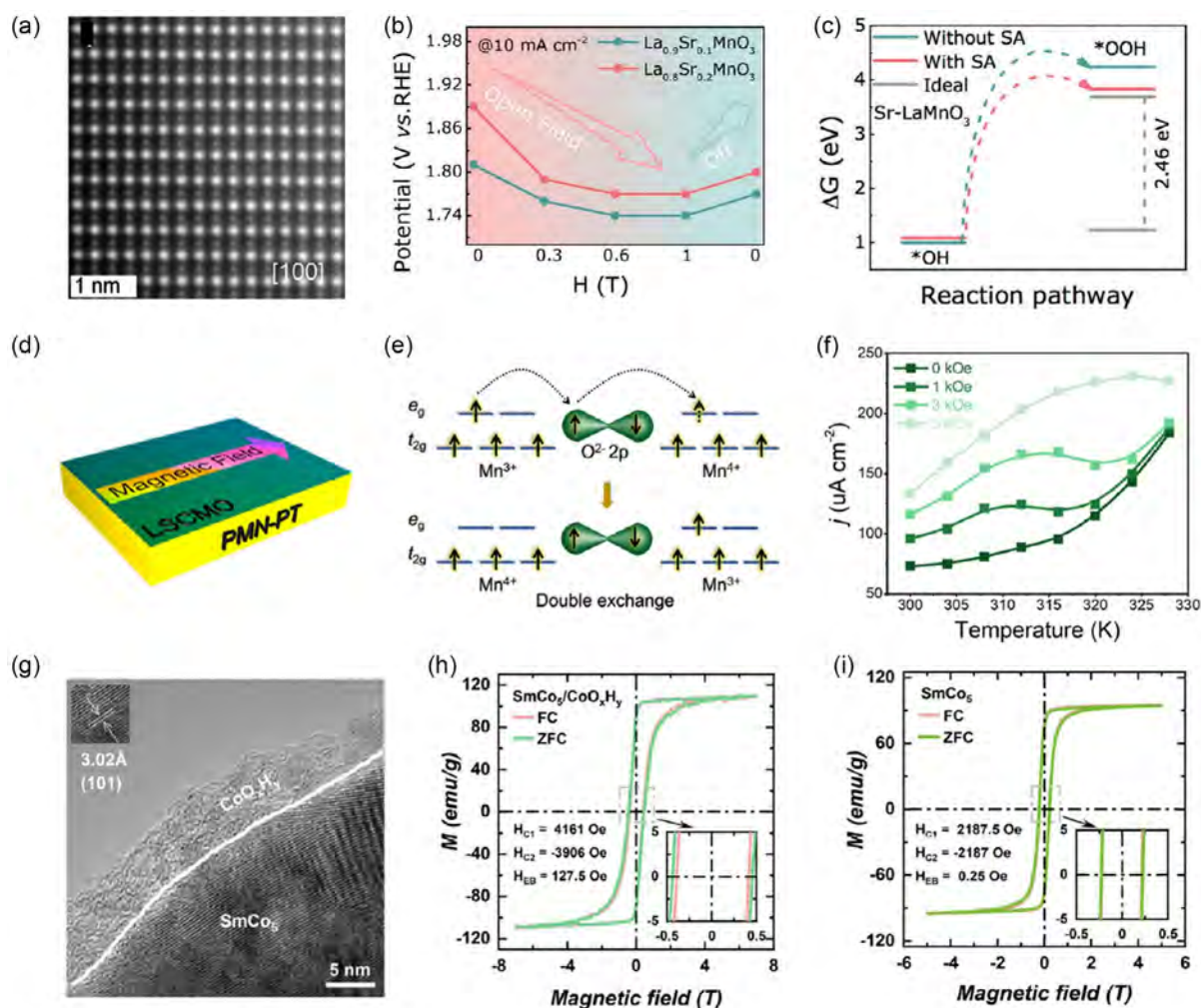

Figure 11. a) High-angle annular dark-field STEM (HAADF-STEM) image of $La_{0.9}Sr_{0.1}MnO_3$ along [100] axis. b) Comparison of potentials achieved at 10 mA cm^{-2} for $La_{0.9}Sr_{0.1}MnO_3$ and $La_{0.8}Sr_{0.2}MnO_3$ under a magnetic field of various field intensities. c) Energy barriers of the transformation from *OH to *OOH for $La_{0.9}Sr_{0.1}MnO_3$ with and without spin alignment. Reproduced with permission.[140] Copyright 2023, Wiley-VCH. d) Schematic illustration of $La_{0.9}Sr_{0.1}MnO_3$ thin film on PMN-PT substrate. e) Process of double exchange in $La_{0.7}Sr_{0.2}Ca_{0.1}MnO_3$. f) Relationship between current density and temperature of $La_{0.7}Sr_{0.2}Ca_{0.1}MnO_3$ under magnetic fields of various field intensity. Reproduced with permission.[141] Copyright 2023, American Chemical Society. g) TEM image of the $SmCo_5/CoO_xH_y$ core/shell particle. The M–H loops of h) $SmCo_5/CoO_xH_y$ and i) $SmCo_5$ under field-cooled and zero-field-cooled modes. Reproduced with permission.[59] Copyright 2021, Wiley-VCH.

activity of $La_{0.7}Sr_{0.2}Ca_{0.1}MnO_3$ exhibits a volcano-shaped trend (Figure 11f), attributed to the coupling of magnetoresistance and spin-polarization effects. Specifically, the magnetoresistance effect is weakened with the increasing temperature so that the charge-transfer resistance of $La_{0.7}Sr_{0.2}Ca_{0.1}MnO_3$ will increase, adversely affecting its catalytic activity. Meanwhile, the effect of spin-polarization-assisted OER by spin-selective electron transfer on Mn sites will also be negatively influenced owing to the more disordered spin direction by thermal disturbance. However, these two passive impacts can be covered by reducing the electrodynamic potential of OER as temperature rises, and the stronger intensity of applying a magnetic field will lead to a higher critical temperature when the current density achieves its maximum. Therefore, magnetoresistance and spin-polarization effects are demonstrated by controlling the reaction temperature within $La_{0.7}Sr_{0.2}Ca_{0.1}MnO_3$.

4.3. Multiple Magnetic Composites

The construction of composite materials promises to integrate the targeted properties of each component, which can develop spin-selective catalysts with both activity, conductivity, and spin polarization. The common strategy is the construction of heterostructure with different magnetic properties. In the following section, the cutting-edge multiple magnetic composites as spin-selective catalysts will be introduced by the order of FM–PM coupling, FM–AFM coupling, and PM–AFM coupling.

4.3.1. FM–PM Coupling

Surficial reconstruction during the electrolytic OER and ORR process will generate highly efficient oxygen-involved intermediates as reaction-preferred species on the surface of transitional metal-based catalysts.[142,143] In recent years, research on surficial reconstruction concentrated on the dynamic evolution of surface morphology[144] and the methods to promote surface reconstruction.[145] As a typical example, Xu et al. prepared PM CoO_xH_y as an active layer on the surface of FM $SmCo_5$ to form a FM–PM heterostructure with robust interfacial spin pinning (Figure 11g).[59] The interfacial magnetic coupling can be reflected by comparing the hysteresis loops of pure $SmCo_5$ and $SmCo_5/CoO_xH_y$ (Figure 11h,i). The spin pinning at the $SmCo_5/CoO_xH_y$ interface is demonstrated by its higher exchange bias (H_{EB}) than pure $SmCo_5$. This H_{EB} arises from uncompensated spins at the interface that cannot fully align with the applied magnetic field,[60,146] which means stronger spin spinning will lead to a larger exchange bias. The as-prepared $SmCo_5/CoO_xH_y$ shows outstanding intrinsic OER catalytic activity in the presence of a magnetic field, and this enhancement by spin polarization can be further influenced by temperature. The impact on the current density increment from temperature is attributed to the fact that higher temperature will weaken the spin pinning effect via perturbing the spin direction of the CoO_xH_y layer, in which case the spin-selective electron transfer on the spin-polarized sites will be limited, thereby elevating the energy barrier of OER. Analogously, Xu et al. reported another material as $CoFe_2O_4/Co(Fe)O_xH_y$ with $CoFe_2O_4$ acting as a FM substrate and the reconstructed oxyhydroxide $Co(Fe)O_xH_y$ acting as the surficial active layer, in which case the intrinsic activity of surficial active sites can be further enhanced by inducing spin-selective electron transfer.[61]

4.3.2. FM–AFM Coupling

Owing to the distinct requirement on magnetic ordering within lattice to form AFM materials, the surface reconstructed hydroxides for FM–PM coupling are not likely to be AFM as they are usually amorphous rather than long-range ordered structures. Therefore, to form FM–AFM coupling at the interface, the materials for different layers need to be carefully selected. Xu et al. investigated the role of FM–AFM coupling in spin-polarization-assisted OER performance by preparing $Fe_3O_4/Ni(OH)_2$ core–shell structure (Figure 12a).[60] Noticeably, with the increasing thickness of the active layer on the surface from 0 to 43 nm, the core–shell structure exhibits varying FM behavior. The coercivity gradually increases while the saturation magnetic moment reduces (Figure 12b). The thicker active layer will lead to stronger FM–AFM coupling at the interface and block the FM signal from the nuclear layer. The $Fe_3O_4/Ni(OH)_2$ with different thicknesses of AFM layers exhibit a volcano-shaped tendency in increasing current density via applying a magnetic field (Figure 12c). This is because if the shell is too thick, the intermediates cannot be absorbed in the FM–AFM coupling interface, thus weakening the effect of spin-selective electron transfer with a magnetic field. Apart from controlling the thickness of the shell, the particle size of the Fe_3O_4 core is also tunable. When the Fe_3O_4 particles are small enough to be single-domain materials, the enhancement from the magnetic field will be negligible, which is in agreement with the case of $CoFe_2O_4$, as reviewed above.

4.3.3. PM–AFM Coupling

Unlike FM–PM and FM–AFM coupling, spin pinning cannot happen at the PM–AFM coupling interface since neither the PM nor AFM layers can exhibit FM behavior under magnetization. Nevertheless, it is possible to induce spin polarization through the spin-exchange interaction between interlayer transition metal elements owing to the strong coupling among lattice structure, electronic orbit, and electron spin.[76] As reported by Tao et al. the interfacial double exchange interaction is introduced between AFM Co_3O_4 and PM NiFe–LDH to generate spin-polarized active sites for conducting spin-selective electron transfer in OER.[62] The magnetization hysteresis ($M–H$) loops of Co_3O_4, NiFe–LDH, and Co3O4@NiFe–LDH demonstrate their respective magnetism. Their intrinsic OER catalytic activity is compared by the normalized current density, in which case the FM Co_3O_4@NiFe–LDH significantly improves catalytic activity compared to the other two samples (Figure 12d,e). The Co, Fe, and Ni sites are spin-polarized by the interfacial FM exchange interaction. Hence, removing electrons from these sites is spin-selective, benefiting the generation of triplet O_2 (Figure 12f,g). Through theoretical calculations, the evolution of *O to *OOH is the rate-determined reaction step, and Co_3O_4@NiFe–LDH has the lower energy barrier for this step (Figure 12h), which is in agreement with its best intrinsic activity among all the tested samples.
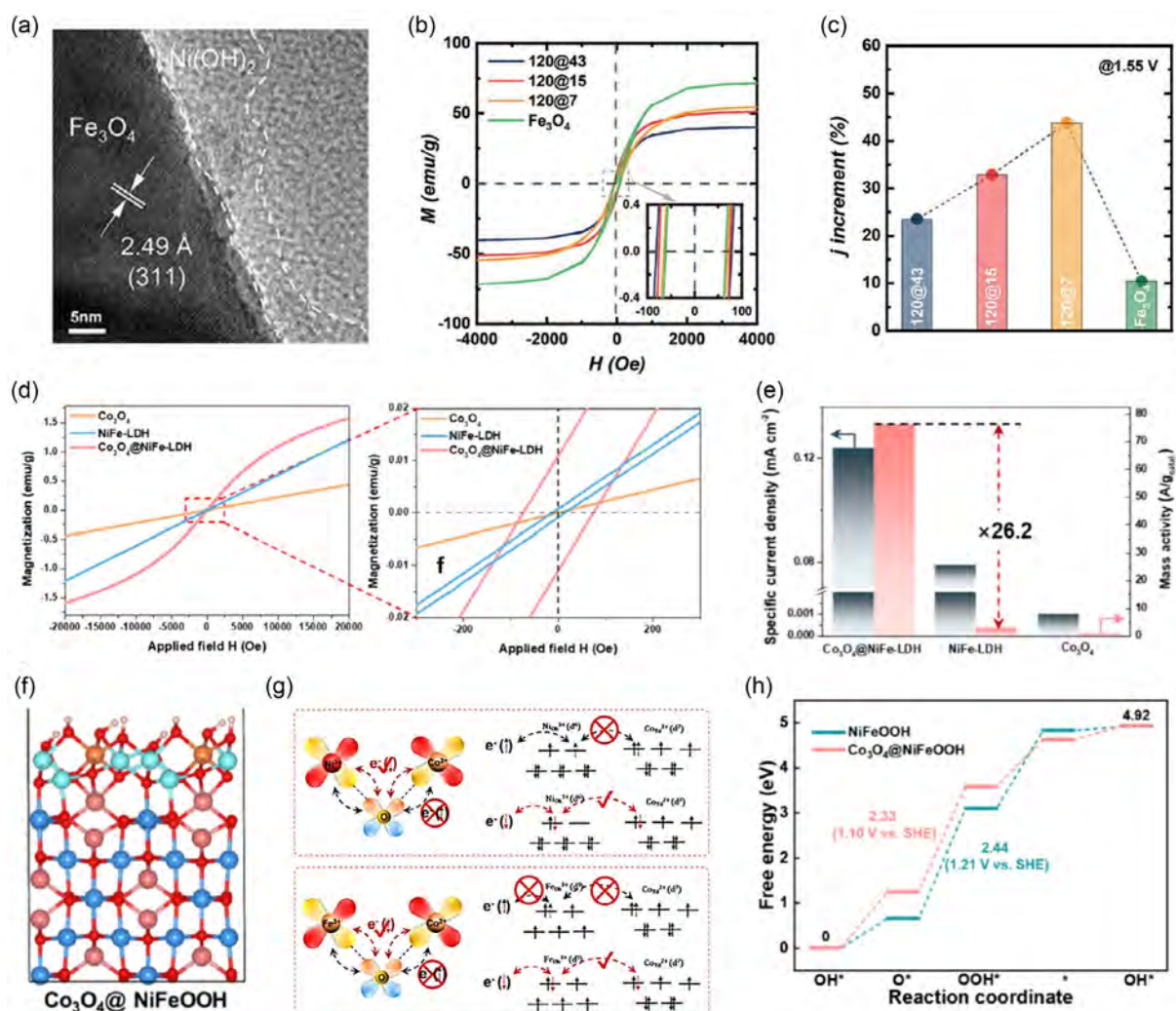
**ADVANCED
SCIENCE NEWS**

www.advancedsciencenews.com

**ADVANCED
ENERGY & SUSTAINABILITY
RESEARCH**

www.advenergysustres.com

Figure 12. a) Representative high-resolution TEM (HRTEM) image of $Fe_3O_4/Ni(OH)_2$ core–shell structure. b) The $M–H$ loops of 120 nm Fe_3O_4 nanoparticles with a thickness of 0, 7, 15, and 43 nm $Ni(OH)_2$ layers. c) Increasement of current density under the magnetic field for 120 nm Fe_3O_4 nanoparticles with a thickness of 0, 7, 15, and 43 nm $Ni(OH)_2$ layers. Reproduced with permission.[60] Copyright 2021, Wiley-VCH. d) The $M–H$ loops of Co_3O_4, NiFe–LDH, and $Co_3O_4@NiFe–LDH$. e) Comparison of OER activity of Co_3O_4, NiFe–LDH, and $Co_3O_4@NiFe–LDH$. f) Lattice structure model of $Co_3O_4@NiFe–LDH$. g) Schematic illustration of spin-selective reaction pathways of $Co_3O_4@NiFe–LDH$. h) Gibbs free energy plots of NiFe–LDH and $Co_3O_4@NiFe–LDH$. Reproduced with permission.[62] Copyright 2024, American Chemical Society.

5. Conclusion and Perspectives

This review highlights recent progress in developing highly efficient spin-selective catalysts from the perspectives of principles, approaches, and research cases, aiming to offer a clear route for designing novel and highly efficient spin-polarized oxygen-involved electrocatalysis. Starting from the fundamental spin-sensitive process in oxygen-involved reaction pathways, the basic requirement and challenge for developing spin-selective catalysts are the existence of spin-polarized active sites. Subsequently, it delves into methodologies for probing the spin-selective mechanism by scrutinizing the application of in situ experimental technologies and theoretical calculations in catalytic mechanism research. Then, as categorized into intrinsic spin-polarized materials, doping-induced spin-polarized materials, and multiple

magnetic composites, the applications of state-of-the-art spin-selective catalysts in electrocatalysis and their mechanism of polarization are systematically reviewed from the perspectives of atomic spin modulation and structural magnetism coupling. This spin-related strategy opens up a new diagram in spin-related energy conversion and enables more efficient use of green energy. Despite significant efforts directed toward the advancement and utilization of spin-selective catalysts, there are still some open questions to be explored, including but not limited to the following.

5.1. Experimental Evidence of Spin-Selective Electron Transfer

To date, the spin-selective electron transfer within OER and ORR is depicted by theoretical calculation, and the in situ

characterization technology has not been widespread for directly observing the evolution of spin states for absorbate and active sites. There are two main questions for realizing the above in situ characterization to obtain reliable data. On the one hand, owing to the robust coupling among spin, orbits, charge, and lattice of transition metal-based compounds, manipulating the spin ordering of catalysts without affecting their other properties can be challenging. On the other hand, integrating magnetic field generators with other equipment is difficult owing to the significant impact of electromagnetic interference on instrument testing. Therefore, a lot of effort should be paid to developing multifield coupling electrochemical in situ characterization equipment, which can not only provide experimental evidence of spin-selective electron transfer but also contribute to deep insights for understanding the structure–property relationship between magnetic structure and electrocatalytic activity. In future research, the challenges of integrating a magnetic field generator into in situ characterization equipment prompt a dual-pronged approach to advancing spin-selective catalyst development. First, by focusing on developing single-domain FM materials, researchers can create spin polarization sites capable of inducing a spin selection effect without an external magnetic field. Notably, many studies rely on magnetic fields generated through electric energy consumption, a practice that undermines overall energy conversion efficiency. Second, efforts can be directed toward enhancing coercive force, particularly in hard magnetic and permanent magnetic materials, by controlling material or element size. This enhancement would enable these materials to maintain a magnetic moment after removing an applied magnetic field, facilitating precharacterization magnetization for subsequent in situ analysis.

5.2. Design of Spin-Selective Catalysts toward Ampere-Level Current Density

The critical demands on developing electrocatalysts serving ampere-level current density have attracted much attention, and the designing strategies from different perspectives are proposed, such as mass transfer capacity, activity, durability, conductivity, and so on. Additionally, given the beneficial effects of Lorentz force and Kelvin force on the release of O_2 bubbles, it is anticipated that the enhancement of OER efficiency through magnetic field assistance will be more pronounced at higher current densities. However, developing room-temperature FM metals with coupled spin polarization and metallicity has always been challenging, not to mention the additional requirements for serving ampere-level current density in harsh environments. In future studies, creating a hierarchical structure represents a promising solution for integrating multiple functions with an ideal electronic and geometric configuration, enhancing electrocatalytic performance. In addition, as discussed in the section on coupled spin-polarized materials, establishing a materials framework with a hierarchical spin-polarized structure is promising to simultaneously obtain outperforming catalytic properties and the integration of various spin-polarization effects, which is meaningful for both practical application and mechanism exploration.

5.3. Relationship between Magnetic Properties and Intrinsic Catalytic Activity

As reviewed in the above sections, various magnetic properties have been demonstrated to be strongly related to the catalytic performance of spin-selective catalysts, such as saturation magnetic moment, coercivity, area of magnetic domain wall, and spin quantum number. However, distinct from the volcano-shaped tendency observed in perovskite and spinel oxides (e.g., the relationship between, e.g., occupation and activity), a universal model between the magnetic properties and the intrinsic catalytic activity has not been established yet. For instance, the positive correlation between saturation moment and activity enhancement is a common tendency for various FM electrocatalysts, as investigated by Galán-Mascarós et al.[22] However, in the cases of single-atom catalysts, researchers have found that the atomic magnetic moment, as modulated by controlling the spin state of a single atom, exhibits a nonmonotonic relation with the resultant catalytic activity. This is because too strong or weak adsorption of intermediates is harmful to the reaction kinetics, and the adsorption of intermediates is related to the charge density distribution, which is sensitive to the spin state of active sites. Therefore, advancing in this research domain requires a deeper elucidation of the correlation between the inherent catalytic activity of spin-selective catalysts and their magnetic moment alongside other magnetic characteristics. Discussions concerning the catalytic efficacy of these catalysts should center on descriptors that can evaluate the intrinsic activity, such as TOF and current density calibrated by the electrochemical active area. The precise understanding of how the intrinsic catalytic performance of spin-selective catalysts relates to their magnetic attributes is paramount for the establishment of accurate material databases for artificial intelligence. Depending on erroneous data for decision-making may result in unfavorable consequences, misdirecting researchers and impeding scientific advancement, innovation, and breakthroughs.

5.4. High-Throughput Experiments and Calculations

The integration of high-throughput experimentation and computational methods is paramount in advancing scarce novel room-temperature FM materials. This combined approach enables rapid screening of numerous samples, expediting the identification of promising candidates, while computational models offer precise predictions on structure–property relationships at the atomic level. For instance, in the section on induced spin-polarized materials, we provided some noble-metal-based spin–selective catalysts with their ferromagnetism induced by $3d$–$5d$ and $3d$–$4d$ orbital interaction. Through machine learning and deep learning technologies, AI can expedite the catalyst design by identifying optimal structures for spin-selective catalysts from vast data. Intelligent algorithms can help predict catalyst performance, optimize reaction conditions, and offer customized solutions, driving innovation in spin-selective catalysts. The application of artificial intelligence will significantly shorten development cycles, reduce costs, and provide more efficient and sustainable solutions for areas such as green energy conversion. In future research endeavors, leveraging AI-powered

high-throughput computational methods will enable swift navigation through all conceivable binary, ternary, and high-entropy combinations. Inducing ferromagnetism within noble-metal compounds to integrate the superiority of these conventional noble-metal catalysts and the spin-polarization effect is a promising pathway toward highly efficient spin-selective catalysts. It is believed that beyond the identified Mn–RuO_2 and CoIr systems, potentially more effective spin-selective catalysts are waiting to be uncovered owing to the nature of robust electron-electron and spin-orbital interactions for $4d$ and $5d$ noble-metal elements. These dual high-throughput strategies accelerate development and provide a comprehensive understanding crucial for innovating room-temperature FM materials into highly efficient spin-selective catalysts by rapidly optimizing designs and delving into the depths of spin-polarization mechanisms.

As a new research area in electrocatalysis, the development of spin-selective catalysts based on spin-polarized materials has great potential in energy conversation while its application- and mechanism-oriented research are still in the early stages. Owing to this field's interdisciplinary nature, advancing spin-related electrocatalysis demands collaborative efforts combining theoretical calculations and advanced technical characterization from various researchers across disciplines like material science, chemistry, physics, and engineering. We believe the advancement of spin-selective catalysts contributes to industrial-level electrochemical application and provides insights for designing room-temperature FM metals facing the challenges in magneto-electric coupling devices.

Acknowledgements

Conflict of Interest

The authors declare no conflict of interest.

Author Contributions

Haifan Li: data curation (lead); formal analysis (lead); writing—original draft (lead); writing—review and editing (supporting). **Quan Quan**: data curation (supporting); formal analysis (supporting); writing—original draft (supporting); writing—review and editing (supporting). **Chun-Yuen Wong**: funding acquisition (supporting); supervision (supporting); writing—review and editing (supporting). **Johnny C. Ho**: funding acquisition (lead); supervision (lead); writing—original draft (supporting); writing—review and editing (lead).

Keywords

[1] C. Wei, R. R. Rao, J. Peng, B. Huang, I. E. L. Stephens, M. Risch, Z. J. Xu, Y. Shao-Horn, *Adv. Mater.* **2019**, *31*, 1806296.
[2] Z. W. Seh, J. Kibsgaard, C. F. Dickens, I. Chorkendorff, J. K. Nørskov, T. F. Jaramillo, *Science* **2017**, *355*, eaad4998.
[3] Q. Quan, J. C. Ho, *Adv. Energy Sustainability Res.* **2022**, *3*, 2200059.
[4] Z. Chen, L. Guo, L. Pan, T. Yan, Z. He, Y. Li, C. Shi, Z.-F. Huang, X. Zhang, J.-J. Zou, *Adv. Energy Mater.* **2022**, *12*, 2103670.
[5] J. Han, J. Sun, S. Chen, S. Zhang, L. Qi, A. Husile, J. Guan, *Adv. Mater.* **2024**, *36*, 2408139.
[6] L. Xiao, L. Qi, J. Sun, A. Husile, S. Zhang, Z. Wang, J. Guan, *Nano Energy* **2024**, *120*, 109155.
[7] F. Cheng, J. Chen, *Chem. Soc. Rev.* **2012**, *41*, 2172.
[8] R. Cao, J.-S. Lee, M. Liu, J. Cho, *Adv. Energy Mater.* **2012**, *2*, 816.
[9] H.-F. Wang, C. Tang, Q. Zhang, *Adv. Funct. Mater.* **2018**, *28*, 1803329.
[10] M. K. Debe, *Nature* **2012**, *486*, 43.
[11] X. X. Wang, M. T. Swihart, G. Wu, *Nat. Catal.* **2019**, *2*, 578.
[12] Y. J. Wang, N. N. Zhao, B. Z. Fang, H. Li, X. T. T. Bi, H. J. Wang, *Chem. Rev.* **2015**, *115*, 3433.
[13] C. Wei, R. R. Rao, J. Y. Peng, B. T. Huang, I. E. L. Stephens, M. Risch, Z. C. J. Xu, Y. Shao-Horn, *Adv. Mater.* **2019**, *31*, 1806296.
[14] J. K. Nørskov, J. Rossmeisl, A. Logadottir, L. Lindqvist, J. R. Kitchin, T. Bligaard, H. Jónsson, *J. Phys. Chem. B* **2004**, *108*, 17886.
[15] J. O. M. Bockris, T. Otagawa, *J. Electrochem. Soc.* **1984**, *131*, 290.
[16] A. Grimaud, K. J. May, C. E. Carlton, Y.-L. Lee, M. Risch, W. T. Hong, J. Zhou, Y. Shao-Horn, *Nat. Commun.* **2013**, *4*, 2439.
[17] F. H. B. D. Lima, J. Zhang, M. Shao, K. Sasaki, M. Vukmirovic, E. A. Ticianelli, R. Adzic, *J. Phys. Chem. C* **2007**, *111*, 404.
[18] J. Suntivich, K. J. May, H. A. Gasteiger, J. B. Goodenough, Y. Shao-Horn, *Science* **2011**, *334*, 1383.
[19] M.-J. Choi, L. Wang, K. A. Stoerzinger, S.-Y. Chung, S. A. Chambers, Y. Du, *Adv. Energy Mater.* **2023**, *13*, 2300239.
[20] J. Suntivich, W. T. Hong, Y.-L. Lee, J. M. Rondinelli, W. Yang, J. B. Goodenough, B. Dabrowski, J. W. Freeland, Y. Shao-Horn, *J. Phys. Chem. C* **2014**, *118*, 1856.
[21] W. T. Hong, K. A. Stoerzinger, Y.-L. Lee, L. Giordano, A. Grimaud, A. M. Johnson, J. Hwang, E. J. Crumlin, W. Yang, Y. Shao-Horn, *Energy Environ. Sci.* **2017**, *10*, 2190.
[22] F. A. Garcés-Pineda, M. Blasco-Ahicart, D. Nieto-Castro, N. López, J. R. Galán-Mascarós, *Nat. Energy* **2019**, *4*, 519.
[23] X. Ren, T. Wu, Y. Sun, Y. Li, G. Xian, X. Liu, C. Shen, J. Gracia, H.-J. Gao, H. Yang, Z. J. Xu, *Nat. Commun.* **2021**, *12*, 2608.
[24] Z. Fang, W. Zhao, T. Shen, D. Qiu, Y. Lv, X. Hou, Y. Hou, *Precis. Chem.* **2023**, *1*, 395.
[25] T. W. Wu, Z. J. Xu, *Curr. Opin. Electrochem.* **2021**, *30*, 100804.
[26] X. Li, Z. Cheng, X. Wang, *Electrochem. Energy Rev.* **2021**, *4*, 136.
[27] Y. Sun, S. Sun, H. Yang, S. Xi, J. Gracia, Z. J. Xu, *Adv. Mater.* **2020**, *32*, 2003297.
[28] J. Gracia, *J. Phys. Chem. C* **2019**, *123*, 9967.
[29] J. Gracia, R. Sharpe, J. Munarriz, *J. Catal.* **2018**, *361*, 331.
[30] J. Gracia, *Phys. Chem. Chem. Phys.* **2017**, *19*, 20451.
[31] Q. Xue, Y. Wang, M. Jiang, R. Cheng, K. Li, T. Zhao, C. Fu, *ACS Appl. Energy Mater.* **2023**, *6*, 1888.
[32] T. Sun, Z. Tang, W. Zang, Z. Li, J. Li, Z. Li, L. Cao, J. S. Dominic Rodriguez, C. O. M. Mariano, H. Xu, P. Lyu, X. Hai, H. Lin, X. Sheng, J. Shi, Y. Zheng, Y.-R. Lu, Q. He, J. Chen, K. S. Novoselov, C.-H. Chuang, S. Xi, X. Luo, J. Lu, *Nat. Nanotechnol.* **2023**, *18*, 763.
[33] J. Ge, X. Ren, R. R. Chen, Y. Sun, T. Wu, S. J. H. Ong, Z. J. Xu, *Angew. Chem., Int. Ed.* **2023**, *62*, e202301721.
[34] Z. Sun, L. Lin, J. He, D. Ding, T. Wang, J. Li, M. Li, Y. Liu, Y. Li, M. Yuan, B. Huang, H. Li, G. Sun, *J. Am. Chem. Soc.* **2022**, *144*, 8204.

[35] Z. Li, Z. Wang, S. Xi, X. Zhao, T. Sun, J. Li, W. Yu, H. Xu, T. S. Herng, X. Hai, P. Lyu, M. Zhao, S. J. Pennycook, J. Ding, H. Xiao, J. Lu, *ACS Nano* **2021**, *15*, 7105.

[36] J. Zhang, S. Shen, D. Puggioni, M. Wang, H. Sha, X. Xu, Y. Lyu, H. Peng, W. Xing, L. N. Walters, L. Liu, Y. Wang, D. Hou, C. Xi, L. Pi, H. Ishizuka, Y. Kotani, M. Kimata, H. Nojiri, T. Nakamura, T. Liang, D. Yi, T. Nan, J. Zang, Z. Sheng, Q. He, S. Zhou, N. Nagaosa, C.-W. Nan, Y. Tokura, R. Yu, J. M. Rondinelli, P. Yu, *Nat. Mater.* **2024**, *23*, 912.

[37] S. Ma, Q. Fu, J. Han, T. Yao, X. Wang, Z. Zhang, P. Xu, B. Song, *Adv. Funct. Mater.* **2024**, *34*, 2316544.

[38] D. Shao, T. Wu, X. Li, X. Ren, Z. J. Xu, *Small Sci.* **2023**, *3*, 2300065.

[39] B. Friedrich, D. Herschbach, *Phys. Today* **2003**, *56*, 53.

[40] P. A. M. Dirac, *Proc. R. Soc. A* **1936**, *155*, 447.

[41] A. L. Buchachenko, V. L. Berdinsky, *Chem. Rev.* **2002**, *102*, 603.

[42] S. Chrétien, H. Metiu, *J. Chem. Phys.* **2008**, *129*, 074705.

[43] E. Torun, C. M. Fang, G. A. de Wijs, R. A. de Groot, *J. Phys. Chem. C* **2013**, *117*, 6353.

[44] Y. Otani, M. Shiraishi, A. Oiwa, E. Saitoh, S. Murakami, *Nat. Phys.* **2017**, *13*, 829.

[45] V.-H. Do, J.-M. Lee, *ACS Nano* **2022**, *16*, 17847.

[46] Y. A. Izyumov, *Phys.-Usp.* **1995**, *38*, 385.

[47] Y. Zhang, Q. Wu, J. Z. Y. Seow, Y. Jia, X. Ren, Z. J. Xu, *Chem. Soc. Rev.* **2024**, *53*, 8123.

[48] T. Reier, H. N. Nong, D. Teschner, R. Schlögl, P. Strasser, *Adv. Energy Mater.* **2017**, *7*, 1601275.

[49] J. S. Yoo, X. Rong, Y. Liu, A. M. Kolpak, *ACS Catal.* **2018**, *8*, 4628.

[50] A. Grimaud, O. Diaz-Morales, B. Han, W. T. Hong, Y.-L. Lee, L. Giordano, K. A. Stoerzinger, M. T. M. Koper, Y. Shao-Horn, *Nat. Chem.* **2017**, *9*, 457.

[51] M. J. Craig, G. Coulter, E. Dolan, J. Soriano-López, E. Mates-Torres, W. Schmitt, M. García-Melchor, *Nat. Commun.* **2019**, *10*, 4993.

[52] J. Rossmeisl, Z. W. Qu, H. Zhu, G. J. Kroes, J. K. Nørskov, *J. Electroanal. Chem.* **2007**, *607*, 83.

[53] Y. Jiao, R. Sharpe, T. Lim, J. W. H. Niemantsverdriet, J. Gracia, *J. Am. Chem. Soc.* **2017**, *139*, 16604.

[54] F. Lyu, Q. Wang, S. M. Choi, Y. Yin, *Small* **2019**, *15*, 1804201.

[55] Q. Shi, C. Zhu, D. Du, Y. Lin, *Chem. Soc. Rev.* **2019**, *48*, 3181.

[56] L. Tan, X. Wu, H. Wang, J. Zeng, B. Mei, X. Pan, W. Hu, M. Faiza, Q. Xiao, Y. Zhao, C. Fu, C. Lin, X. Li, W. Luo, *ACS Catal.* **2024**, *14*, 11273.

[57] L. Li, Y. Wang, R. R. Nazmutdinov, R. R. Zairov, Q. Shao, J. Lu, *Nano Lett.* **2024**, *24*, 6148.

[58] L. Li, J. Zhou, X. Wang, J. Gracia, M. Valvidares, J. Ke, M. Fang, C. Shen, J.-M. Chen, Y.-C. Chang, C.-W. Pao, S.-Y. Hsu, J.-F. Lee, A. Ruotolo, Y. Chin, Z. Hu, X. Huang, Q. Shao, *Adv. Mater.* **2023**, *35*, 2302966.

[59] R. R. Chen, G. Chen, X. Ren, J. Ge, S. J. H. Ong, S. Xi, X. Wang, Z. J. Xu, *Angew. Chem., Int. Ed.* **2021**, *60*, 25884.

[60] J. Ge, R. R. Chen, X. Ren, J. Liu, S. J. H. Ong, Z. J. Xu, *Adv. Mater.* **2021**, *33*, 2101091.

[61] T. Wu, X. Ren, Y. Sun, S. Sun, G. Xian, G. G. Scherer, A. C. Fisher, D. Mandler, J. W. Ager, A. Grimaud, J. Wang, C. Shen, H. Yang, J. Gracia, H.-J. Gao, Z. J. Xu, *Nat. Commun.* **2021**, *12*, 3634.

[62] Z. Xue, B. Wu, Z. Zhang, C. Lin, X. Li, Q. Zhang, K. Tao, *ACS Catal.* **2024**, *14*, 5685.

[63] F. de Groot, *Chem. Rev.* **2001**, *101*, 1779.

[64] W. H. Lee, M. H. Han, Y.-J. Ko, B. K. Min, K. H. Chae, H.-S. Oh, *Nat. Commun.* **2022**, *13*, 605.

[65] H. Jia, N. Yao, Z. Liao, L. Wu, J. Zhu, Y. Lao, W. Luo, *Angew. Chem., Int. Ed.* **2024**, *63*, e202408005.

[66] F. Attar, H. Yin, S. L. Schumann, J. Langley, N. Cox, Z. Zeng, K. Catchpole, S. Karuturi, Z. Yin, *Energy Environ. Sci.* **2024**, *17*, 3307.

[67] D. Hollmann, N. Rockstroh, K. Grabow, U. Bentrup, J. Rabeah, M. Polyakov, A.-E. Surkus, W. Schuhmann, S. Hoch, A. Brückner, *ChemElectroChem* **2017**, *4*, 2117.

[68] Y. Kutin, N. Cox, W. Lubitz, A. Schnegg, O. Rüdiger, *Catalysts* **2019**, *9*, 926.

[69] T. E. Cranshaw, *J. Phys. E: Sci. Instrum.* **1974**, *7*, 497.

[70] J. Y. C. Chen, L. Dang, H. Liang, W. Bi, J. B. Gerken, S. Jin, E. E. Alp, S. S. Stahl, *J. Am. Chem. Soc.* **2015**, *137*, 15090.

[71] Q. Xie, D. Ren, L. Bai, R. Ge, W. Zhou, L. Bai, W. Xie, J. Wang, M. Grätzel, J. Luo, *Chin. J. Catal.* **2023**, *44*, 127.

[72] X. Liao, R. Lu, L. Xia, Q. Liu, H. Wang, K. Zhao, Z. Wang, Y. Zhao, *Energy Environ. Mater.* **2022**, *5*, 157.

[73] R. R. Chen, Y. Sun, S. J. H. Ong, S. Xi, Y. Du, C. Liu, O. Lev, Z. J. Xu, *Adv. Mater.* **2020**, *32*, 1907976.

[74] Y. Wang, P. Meng, Z. Yang, M. Jiang, J. Yang, H. Li, J. Zhang, B. Sun, C. Fu, *Angew. Chem., Int. Ed.* **2023**, *62*, e202304229.

[75] H. Zhang, H.-C. Chen, S. Feizpoor, L. Li, X. Zhang, X. Xu, Z. Zhuang, Z. Li, W. Hu, R. Snyders, D. Wang, C. Wang, *Adv. Mater.* **2024**, *36*, 2400523.

[76] Y. Tokura, N. Nagaosa, *Science* **2000**, *288*, 462.

[77] M. Li, X. Wang, K. Liu, Z. Zhu, H. Guo, M. Li, H. Du, D. Sun, H. Li, K. Huang, Y. Tang, G. Fu, *Adv. Energy Mater.* **2023**, *13*, 2301162.

[78] X. Wang, M. Li, P. Wang, D. Sun, L. Ding, H. Li, Y. Tang, G. Fu, *Small Methods* **2023**, *7*, 2300100.

[79] S. Liu, L. Li, T. Yang, E. Wang, X. Yu, Y. Hou, Z. Du, S. Cao, K.-C. Chou, X. Hou, *J. Mater. Sci. Technol.* **2024**, in press. https://doi.org/10.1016/j.jmst.2024.09.014.

[80] L. Yang, T. Yang, E. Wang, X. Yu, K. Wang, Z. Du, S. Cao, K.-C. Chou, X. Hou, *J. Mater. Sci. Technol.* **2023**, *159*, 33.

[81] T. Heine, *Acc. Chem. Res.* **2015**, *48*, 65.

[82] J. Yin, J. Jin, H. Lin, Z. Yin, J. Li, M. Lu, L. Guo, P. Xi, Y. Tang, C.-H. Yan, *Adv. Sci.* **2020**, *7*, 1903070.

[83] M. Du, X. Li, H. Pang, Q. Xu, *EnergyChem* **2023**, *5*, 100083.

[84] C. Kim, F. Dionigi, V. Beermann, X. Wang, T. Möller, P. Strasser, *Adv. Mater.* **2019**, *31*, 1805617.

[85] E. Antolini, *Appl. Catal., B* **2017**, *217*, 201.

[86] S. Zhang, S. E. Saji, Z. Y. Yin, H. B. Zhang, Y. P. Du, C. H. Yan, *Adv. Mater.* **2021**, *33*, 2005988.

[87] G. Giannakakis, M. Flytzani-Stephanopoulos, E. C. H. Sykes, *Acc. Chem. Res.* **2019**, *52*, 237.

[88] Z. Yang, W. Gao, *Adv. Sci.* **2022**, *9*, 22.

[89] T. J. Zhang, A. G. Walsh, J. H. Yu, P. Zhang, *Chem. Soc. Rev.* **2021**, *50*, 569.

[90] X. Xu, J. Guan, *Chem. Sci.* **2024**, *15*, 14585.

[91] R. Z. Li, D. S. Wang, *Adv. Energy Mater.* **2022**, *12*, 2103564.

[92] J. Wang, C. X. Zhao, J. N. Liu, Y. W. Song, J. Q. Huang, B. Q. Li, *Nano Energy* **2022**, *104*, 107927.

[93] M. Luneau, J. S. Lim, D. A. Patel, E. C. H. Sykes, C. M. Friend, P. Sautet, *Chem. Rev.* **2020**, *120*, 12834.

[94] F. Gao, D. W. Goodman, *Chem. Soc. Rev.* **2012**, *41*, 8009.

[95] T. Tang, J. Han, Z. Wang, X. Niu, J. Guan, *Nano Res.* **2024**, *17*, 3794.

[96] T. Tang, Y. Wang, J. Han, Q. Zhang, X. Bai, X. Niu, Z. Wang, J. Guan, *Chin. J. Catal.* **2023**, *46*, 48.

[97] A. I. Hutu, E. Pervolarakis, I. N. Remediakis, H. H. Kristoffersen, J. Rossmeisl, *J. Phys. Chem. C* **2024**, *128*, 10251.

[98] C. H. Wu, M. H. Jin, D. Y. Guo, L. H. Wu, C. Wang, X. Chen, S. Wang, *Adv. Sustainable Syst.* **2023**, *7*, 2300192.

[99] L. L. Yu, K. Z. Zeng, C. H. Li, X. R. Lin, H. W. Liu, W. H. Shi, H. J. Qiu, Y. F. Yuan, Y. G. Yao, *Carbon Energy* **2022**, *4*, 731.

[100] W. B. Zhang, W. Yuan, X. Q. Zhang, Y. Z. Ke, Y. P. Wu, Y. F. Bai, S. M. Jiang, Y. Tang, *J. Mater. Chem. A* **2024**, *12*, 18705.

[101] W. Kiciński, J. P. Sęk, E. Matysiak-Brynda, K. Miecznikowski, M. Donten, B. Budner, A. M. Nowicka, *Appl. Catal., B* **2019**, *258*, 117955.

[102] X. Li, C. Hao, Y. Du, Y. Lu, Y. Fan, M. Wang, N. Wang, R. Meng, X. Wang, Z. J. Xu, Z. Cheng, *Chin. J. Catal.* **2023**, *55*, 191.

[103] J. Hwang, R. R. Rao, L. Giordano, Y. Katayama, Y. Yu, Y. Shao-Horn, *Science* **2017**, *358*, 751.

[104] K. Saini, A. N. Nair, A. Yadav, L. G. Enriquez, C. J. Pollock, S. D. House, S. Yang, X. Guo, S. T. Sreenivasan, *Adv. Energy Mater.* **2023**, *13*, 2302170.

[105] C. Fang, J. Zhou, L. Zhang, W. Wan, Y. Ding, X. Sun, *Nat. Commun.* **2023**, *14*, 4449.

[106] C. Chen, Y. Li, A. Huang, X. Liu, J. Li, Y. Zhang, Z. Chen, Z. Zhuang, Y. Wu, W.-C. Cheong, X. Tan, K. Sun, Z. Xu, D. Liu, Z. Wang, K. Zhou, C. Chen, *J. Am. Chem. Soc.* **2023**, *145*, 21273.

[107] J. Zhang, Y. Zhao, W. Zhao, J. Wang, Y. Hu, C. Huang, X. Zou, Y. Liu, D. Zhang, X. Lu, H. Fan, Y. Hou, *Angew. Chem., Int. Ed.* **2023**, *62*, e202314303.

[108] Y. Su, X. Ding, J. Yuan, *Int. J. Hydrogen Energy* **2024**, *55*, 893.

[109] X. Ren, T. Wu, Z. Gong, L. Pan, J. Meng, H. Yang, F. B. Dagbjartsdottir, A. Fisher, H.-J. Gao, Z. J. Xu, *Nat. Commun.* **2023**, *14*, 2482.

[110] T. Wu, J. Ge, Q. Wu, X. Ren, F. Meng, J. Wang, S. Xi, X. Wang, K. Elouarzaki, A. Fisher, Z. J. Xu, *Proc. Natl. Acad. Sci.* **2024**, *121*, e2318652121.

[111] Y. Liu, S. Jiang, S. Li, L. Zhou, Z. Li, J. Li, M. Shao, *Appl. Catal., B* **2019**, *247*, 107.

[112] L. Du, G. Shi, Y. Zhao, X. Chen, H. Sun, F. Liu, F. Cheng, W. Xie, *Chem. Sci.* **2019**, *10*, 9605.

[113] Y. Sun, K. Xu, Z. Wei, H. Li, T. Zhang, X. Li, W. Cai, J. Ma, H. J. Fan, Y. Li, *Adv. Mater.* **2018**, *30*, 1802121.

[114] J. Lian, Y. Wu, H. Zhang, S. Gu, Z. Zeng, X. Ye, *Int. J. Hydrogen Energy* **2018**, *43*, 12929.

[115] W. Wan, Y. Zhao, S. Wei, C. A. Triana, J. Li, A. Arcifa, C. S. Allen, R. Cao, G. R. Patzke, *Nat. Commun.* **2021**, *12*, 5589.

[116] Y. Wang, Y. Shang, Z. Cao, Z. Keng, Y. Xie, J. Li, Y. Yao, W. Gan, *Chem. Eng. J.* **2022**, *439*, 135722.

[117] J. Chen, Y. Ling, X. Yu, G. Wang, L. Huang, A. He, Q. Fan, S. Qin, S. Xiang, M. Xu, Z. Han, J. Du, Q. Xu, *J. Alloys Compd.* **2022**, *929*, 167344.

[118] Y. Ma, T. Wang, X. Sun, Y. Yao, H. Chen, G. Wu, C. Zhang, Y. Qin, *ACS Appl. Mater. Interfaces* **2023**, *15*, 7978.

[119] P. Guo, Y. Zhang, F. Han, Y. Du, B. Song, W. Wang, X. Wang, Y. Zhou, P. Xu, *J. Phys. Chem. Lett.* **2022**, *13*, 7476.

[120] Q. Huang, S. Xie, J. Hao, Z. Ding, C. Zhang, H. Sheng, J. Zhao, *Angew. Chem., Int. Ed.* **2023**, *62*, e202300469.

[121] M. Chen, W. Zhou, K. Ye, C. Yuan, M. Zhu, H. Yu, H. Yang, H. Huang, Y. Wu, J. Zhang, X. Zheng, J. Shen, X. Wang, S. Wang, *Small* **2023**, *19*, 2300122.

[122] A. Karn, Y. H. Chan, U. Chazarin, P. Chen, W. W. Pai, *AIP Adv.* **2022**, *12*, 035240.

[123] J. Jiang, R. Li, W. Mi, *Mater. Horiz.* **2022**, *9*, 2785.

[124] D. Li, X. Wang, C.-M. Kan, H. He, Z. Li, Q. Hao, H. Zhao, C. Wu, C. Jin, X. Cui, *ACS Appl. Mater. Interfaces* **2020**, *12*, 25143.

[125] Y. Xue, Y. Zhang, H. Wang, S. Lin, Y. Li, J.-Y. Dai, S. P. Lau, *Nanotechnology* **2020**, *31*, 145712.

[126] C. Li, M. Wei, D. G. Evans, X. Duan, *Catal. Today* **2015**, *247*, 163.

[127] F. Li, H. Ai, D. Liu, K. H. Lo, H. Pan, *J. Mater. Chem. A* **2021**, *9*, 17749.

[128] L. Lin, R. Xin, M. Yuan, T. Wang, J. Li, Y. Xu, X. Xu, M. Li, Y. Du, J. Wang, S. Wang, F. Jiang, W. Wu, C. Lu, B. Huang, Z. Sun, J. Liu, J. He, G. Sun, *ACS Catal.* **2023**, *13*, 1431.

[129] Y. Di, M. Chai, Y. Lv, E. Wang, T. Yang, Z. Fang, X. Hou, *Ceram. Int.* **2024**, *50*, 21937.

[130] H. F. Li, F. Q. Meng, Y. Bian, X. C. Zhou, J. U. Wang, X. G. Xu, Y. Jiang, N. F. Chen, J. K. Chen, *J. Mater. Sci. Technol.* **2023**, *148*, 235.

[131] J. K. Chen, H. Y. Hu, J. O. Wang, C. Liu, X. L. Liu, Z. Li, N. F. Chen, *ACS Appl. Mater. Interfaces* **2019**, *11*, 34128.

[132] J. K. Chen, H. F. Li, J. O. Wang, X. Y. Ke, B. H. Ge, J. H. Chen, H. L. Dong, Y. Jiang, N. F. Chen, *J. Mater. Chem. A* **2020**, *8*, 13630.

[133] Y. F. Sun, T. N. H. Nguyen, A. Anderson, X. Cheng, T. E. Gage, J. Lim, Z. Zhang, H. Zhou, F. Rodolakis, Z. Zhang, I. Arslan, S. Ramanathan, H. Lee, A. A. Chubykin, *ACS Appl. Mater. Interfaces* **2020**, *12*, 24564.

[134] H. T. Zhang, F. Zuo, F. R. Li, H. Chan, Q. Y. Wu, Z. Zhang, B. Narayanan, K. Ramadoss, I. Chakraborty, G. Saha, G. Kamath, K. Roy, H. Zhou, A. A. Chubykin, S. K. R. S. Sankaranarayanan, J. H. Choi, S. Ramanathan, *Nat. Commun.* **2019**, *10*, 1651.

[135] Z. Zhang, D. Schwanz, B. Narayanan, M. Kotiuga, J. A. Dura, M. Cherukara, H. Zhou, J. W. Freeland, J. R. Li, R. Sutarto, F. Z. He, C. Wu, J. X. Zhu, Y. F. Sun, K. Ramadoss, S. S. Nonnenmann, N. F. Yu, R. Comin, K. M. Rabe, S. K. R. S. Sankaranarayanan, S. Ramanathan, *Nature* **2018**, *553*, 68.

[136] H. T. Zhang, T. J. Park, I. A. Zaluzhnyy, Q. Wang, S. N. Wadekar, S. Manna, R. Andrawis, P. O. Sprau, Y. F. Sun, Z. Zhang, C. Z. Huang, H. Zhou, Z. Zhang, B. Narayanan, G. Srinivasan, N. Hua, E. Nazaretski, X. Huang, H. F. Yan, M. Ge, Y. S. Chu, M. J. Cherukara, M. V. Holt, M. Krishnamurthy, O. G. Shpyrko, S. K. R. S. Sankaranarayanan, A. Frano, K. Roy, S. Ramanathan, *Nat. Commun.* **2020**, *11*, 2245.

[137] Y. Zhou, S. Ramanathan, *Crit. Rev. Solid State* **2013**, *38*, 286.

[138] Z. Chen, X. Duan, W. Wei, S. Wang, B.-J. Ni, *Nano Energy* **2020**, *78*, 105270.

[139] V. V. Krishnamurthy, D. J. Singh, N. Kawamura, M. Suzuki, T. Ishikawa, *Phys. Rev. B* **2006**, *74*, 064411.

[140] J. Qian, H. Zhang, G. Li, L. Jia, X. Peng, C. Zhong, F. Li, D. Chao, D. Gao, *Adv. Funct. Mater.* **2024**, *34*, 2305621.

[141] H. Xu, J. Qi, Y. Zhang, H. Liu, L. Hu, M. Feng, W. Lü, *ACS Appl. Mater. Interfaces* **2023**, *15*, 32320.

[142] L. Gao, X. Cui, C. D. Sewell, J. Li, Z. Lin, *Chem. Soc. Rev.* **2021**, *50*, 8428.

[143] Y. Li, X. Du, J. Huang, C. Wu, Y. Sun, G. Zou, C. Yang, J. Xiong, *Small* **2019**, *15*, 1901980.

[144] W. Shen, J. Yin, J. Jin, Y. Hu, Y. Hou, J. Xiao, Y.-Q. Zhao, P. Xi, *Adv. Energy Sustainability Res.* **2022**, *3*, 2200036.

[145] H. Liu, R. Xie, Q. Wang, J. Han, Y. Han, J. Wang, H. Fang, J. Qi, M. Ding, W. Ji, *Adv. Sci.* **2023**, *10*, 2207128.

[146] Q. K. Ong, X.-M. Lin, A. Wei, *J. Phys. Chem. C* **2011**, *115*, 2665.

**ADVANCED
SCIENCE NEWS**

www.advancedsciencenews.com

**ADVANCED
ENERGY & SUSTAINABILITY
RESEARCH**
Open Access

www.advenergysustres.com

Haifan Li is a Ph.D. candidate in the Department of Chemistry at the City University of Hong Kong. His research interests mainly focus on synthesizing spin-polarized catalysts and the hydrogenation-assisted electronic phase transition for applications in electrocatalysis and interdisciplinary sustainable chemistry.

Quan Quan is a postdoctoral researcher in the Department of Materials Science and Engineering at the City University of Hong Kong. Her research interests mainly focus on synthesizing nanostructural catalysts for applications in electrocatalysis and related interdisciplinary sustainable chemistry.

Chun-Yuen Wong is a professor in the Department of Chemistry at the City University of Hong Kong. He received his B.Sc. in 2000 and Ph.D. in 2005 from The University of Hong Kong. He was a Croucher Foundation Postdoctoral Fellow at Harvard University from 2005 to 2006. His current research interests include probing the metal–carbon bonding interactions in organometallic complexes through spectroscopic and theoretical means to provide insight into the design of functional organometallic complexes and designing metal/semiconductor hybrid nanostructures for photonic application.

Johnny C. Ho is a professor in the Department of Materials Science and Engineering at the City University of Hong Kong. He received his B.S. in chemical engineering and his M.S. and Ph.D. in materials science and engineering from the University of California, Berkeley, in 2002, 2005, and 2009, respectively. From 2009 to 2010, he was a postdoctoral research fellow in the Nanoscale Synthesis and Characterization Group at Lawrence Livermore National Laboratory. His research interests focus on nanoscale materials' synthesis, characterization, integration, and device applications for various technological applications, including nanoelectronics, sensors, and energy harvesting.